Article for:
Handbook of Spectroscopy, Vo-Dinh, Gauglitz (eds.), Wiley
In Volume: Methods 2: NMR Spectroscopy

Solid-State NMR

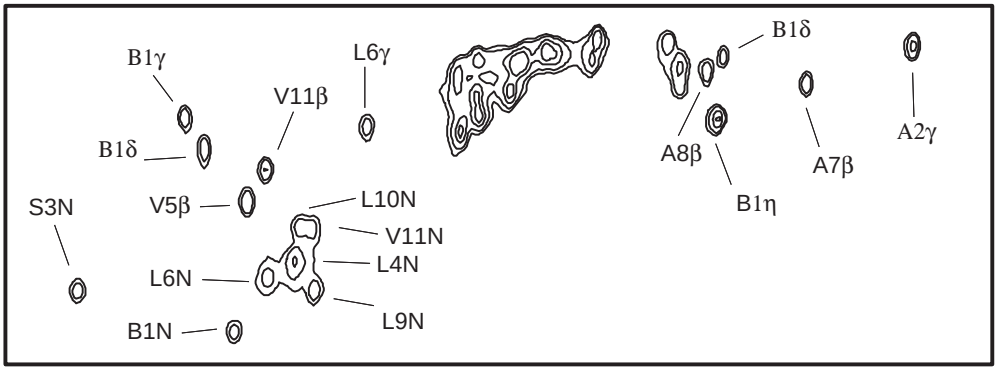

Steven P. Brown and Lyndon Emsley

Laboratoire de Stéréochimie et des Interactions Moléculaires,
Ecole Normale Supérieure de Lyon, 69364 Lyon, France

1 INTRODUCTION

For the chemist today, the importance of solution-state NMR is well established. Individual nuclei within a molecule are differentiated on account of their chemical shift, while connectivities, which permit spectral assignment, are identified by through-bond *J* couplings. Through-space proximities, which yield information about three-dimensional structure, are accessible by experiments which exploit the nuclear Overhauser effect (NOE). Moreover, a host of multi-dimensional experiments have been developed which further enhance the information content.[1,2] In many cases, however, the most appropriate sample to study molecular structure and dynamics is the solid. The purpose of this article is to give an overview of the different solid-state NMR methods which are available in such cases. Our focus is on the structural and dynamic information which a particular method can deliver, and, at most, only a simple qualitative explanation of how the experiment works will be given, although the relevant literature will always be cited, such that the interested reader can find details about, e.g., the experimental implementation.

Firstly, it is necessary to consider how and why NMR of solid samples differs from the solution-state case. High-resolution solution-state spectra are a result of fast isotropic molecular tumbling. In the solid state, this motion is (usually) absent, and anisotropic interactions, i.e., the chemical shift anisotropy (CSA), and the dipolar and quadrupolar couplings, lead to a broadening – see section II – of the resonances.[3-5] These anisotropic interactions, on the one hand, have the significant disadvantage of hindering the resolution of distinct sites, but, on the other hand, contain valuable structural and dynamic information. Specifically, the CSA and quadrupolar interactions provide insight into electronic structure and bonding, while the dipolar coupling offers direct access to internuclear distances. Moreover, all three anisotropic interactions are formidable probes of dynamics. As will be demonstrated in this article a number of ingenious experimental approaches have been developed which provide access to the information inherent to the anisotropic interactions particular to the solid state, while retaining the site specificity associated with high-resolution NMR.

Tables 1 and 2 list the NMR-active nuclei (i.e., those with $I > 0$) of most relevance for organic and inorganic solids, respectively, together with their nuclear spin quantum numbers, their magnetogyric ratios (γ), and natural abundances. (For a comprehensive listing of all NMR-active nuclei, the reader is referred to Ref. [6]) For spin $I = 1/2$ nuclei, the two most important anisotropic interactions are the anisotropy of the chemical shielding interaction and the dipolar coupling between the dipole moments of two or more spins. This is to be compared to the case of nuclei with $I \geq 1$, which possess a quadrupole moment,

Table 1. The properties of the NMR-active nuclei of most relevance for organic solids.[6]

Nucleus	*I*	$\gamma/ 10^7$ rad T^{-1} s^{-1}	Natural Abundance/ %
^{1}H	1/2	26.8	99.99
^{2}H	1	4.1	0.02
^{13}C	1/2	6.7	1.10
^{14}N	1	1.9	99.63
^{15}N	1/2	–2.7	0.37
^{17}O	5/2	–3.6	0.04
^{19}F	1/2	25.2	100.00

Table 2. The properties of the NMR-active nuclei of most relevance for inorganic solids.[6]

Nucleus	*I*	$\gamma/ 10^7$ rad T^{-1} s^{-1}	Natural Abundance/ %
^{6}Li	1	3.9	7.50
^{7}Li	3/2	10.4	92.50
^{11}B	3/2	8.6	80.10
^{17}O	5/2	–3.6	0.04
^{23}Na	3/2	7.1	100.00
^{25}Mg	5/2	–1.6	10.00
^{27}Al	5/2	7.0	100.00
^{29}Si	1/2	–5.3	4.67
^{31}P	1/2	10.8	100.00
^{33}S	3/2	2.1	0.75
^{45}Sc	7/2	6.5	100.00
^{47}Ti	5/2	–1.5	7.30
^{49}Ti	7/2	–1.5	5.50
^{51}V	7/2	7.0	99.75
^{55}Mn	5/2	6.6	100.00
^{59}Co	7/2	6.3	100.00
^{67}Zn	5/2	1.7	4.10
^{71}Ga	3/2	8.2	39.89
^{87}Rb	3/2	8.8	27.83
^{93}Nb	9/2	6.6	100.00
^{113}Cd	1/2	–6.0	12.22
^{119}Sn	1/2	–10.0	8.59
^{133}Cs	7/2	3.5	100.00
^{195}Pt	1/2	5.8	33.80
^{207}Pb	1/2	5.6	22.10

and whose spectra are dominated by the interaction of the quadrupole moment with the electric field gradient at the nucleus. Thus, a separate methodology exists for quadrupolar nuclei. Moreover, it is further necessary to distinguish between quadrupolar nuclei with integer (only I =1) and half-integer spin (I = 3/2. 5/2, 7/2, 9/2), since in the latter case the presence of a "central transition", which is not broadened by the quadrupolar interaction to a first-order approximation modifies the experimental approach. Solid-state NMR methods suitable for half-integer quadrupolar nuclei, e.g. ^{17}O, ^{23}Na, and ^{27}Al, which are of much importance in inorganic systems, are therefore discussed separately in section 7.

Nuclei can be further classified as to their natural abundance: nuclei with 99+ % natural abundance, e.g., ^{1}H, ^{19}F, and ^{31}P, are referred to as being abundant, while nuclei with low natural abundances, e.g. ^{2}H, ^{13}C, and ^{15}N, are termed dilute or rare. For dilute nuclei, there exists the possibility to achieve site selectivity by means of selective isotopic labelling. In an NMR experiment, the sensitivity, i.e., the signal-to-noise ratio (S/N), depends on the natural abundance, i.e., the number of NMR-active nuclei in the sample, as well as the magnetogyric ratio, which determines the Larmor frequency of the nucleus at a particular magnetic field. Of all the naturally occurring nuclei, the proton, ^{1}H, thus, has the best sensitivity. However, unlike in solution-state NMR where ^{1}H NMR is of central importance, in the solid-state there exists a major complication with ^{1}H NMR primarily due to its high natural abundance; namely, the abundance of protons in organic solids means that there exist strongly dipolar-coupled proton networks, which lead to static line broadenings of the order of 50 kHz. As a consequence, as far as organic solids are concerned, attention has rather focused on dilute spin I = 1/2 nuclei, e.g., ^{13}C and ^{15}N. However, as will be discussed briefly in this article, new high-resolution ^{1}H solid-state NMR methods have recently been developed,[7] such that the importance of ^{1}H solid-state NMR is expected to increase significantly in the coming years.

In this article, we will first illustrate how anisotropic interactions lead to a broadening of the NMR resonances (section 2), and then describe the principal line-narrowing method in solid-state NMR, namely magic-angle spinning (MAS), in section 3. As stated above, achieving high-resolution is not the only goal in solid-state NMR, and ideally the spectroscopist would like to combine this with the retention of the structural and dynamic information inherent to the anisotropic interactions responsible for the line broadening. Recoupling methods[8,9] are the subject of section 4. As in solution-state NMR, the extension of the experiment to a second (and higher) dimension is of much importance in solid-state NMR; homonuclear and heteronuclear multi-dimensional experiments are discussed in sections 5 and

6, respectively. Finally, methods applicable to half-integer quadrupolar nuclei are introduced in section 7.

2 SOLID-STATE NMR LINESHAPES

2.1 The Orientational Dependence of the NMR Resonance Frequency

In solid-state NMR, a very important concept is that *the resonance frequency of a given nucleus within a particular crystallite depends on the orientation of the crystallite*.[3-5] Considering the example of the CSA of a ^{13}C nucleus in a carboxyl group, Figure 1 illustrates how the resonance frequency varies for three particular orientations of the molecule with respect to the static magnetic field, B_0. At this point, we note that that the orientation dependence of the CSA, dipolar, and first-order quadrupolar interactions can all be represented by what are referred to as second-rank tensors. This simply means that the interaction can be described mathematically in Cartesian space by a 3×3 matrix (this is to be compared with scalar and vector quantities, which are actually zero- and first- rank tensors, and are specified by a single element and a 3×1 matrix, respectively). For such a second-rank tensor, there exists a principal axes system (PAS) in which only the diagonal elements of the matrix are non-zero. Indeed, the orientations illustrated in Figure 1 correspond to the orientation of the three principal axes of the chemical shift tensor with respect to the axis defined by B_0.

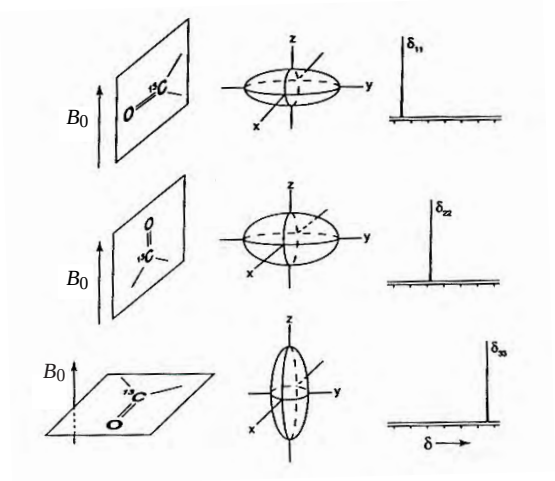

Figure 1. The dependence of the resonance frequency upon orientation for an anisotropic interaction, namely the CSA of a ^{13}C nucleus in a carboxyl group. The orientations illustrated correspond to the alignment of the three principal axes of the chemical shift tensor with the axis defined by B_0. (Reproduced by permission of the Società Italiana di Fisica from Ref. 5.)

To fully characterise the CSA and the first-order quadrupolar coupling, it is necessary to determine the three principal values (corresponding to the diagonal elements in the PAS) as well as the two angles (referred to as Euler angles) which describe the rotation of the PAS onto a fixed reference frame, e.g. that specified by B_0. The mathematical expression for the dependence of the resonance frequency of a given nucleus in a crystallite on these parameters is given in the Appendix. It should be noted that the dipolar coupling between a pair of spins is always axially symmetric, and is fully specified by a single principal value and a single angle (see also the Appendix). Since the principal values and Euler angles for a given anisotropic interaction contain valuable chemical information, e.g., about the electronic environment, one of the

principal aims of solid-state NMR is the development of methods by which these parameters can be determined.

2.2 Single-Crystal NMR

One approach by means of which the principal values and orientations of the different anisotropic interactions can be determined involves the measurement of the change in the observed resonance frequencies upon rotating a single crystal in a well-defined fashion.[10] This is illustrated in Figure 2 for the case of ^{2}H NMR of a single crystal of the peptide *N*-acetyl-D, L-valine (NAV) for which the exchangeable amide and carboxyl hydrogens were deuterated.[11] The quadrupolar coupling leads to an inequivalence of the two single-quantum (SQ) transitions associated with a spin I = 1 nucleus such that a doublet is observed for each distinct deuterium. There are two molecules in the unit cell of NAV, and thus two crystallographically distinct hydrogen positions for both the amide and carboxyl groups, yielding four different deuterons, and therefore eight separate lines are observed (see Figure 2(a)).

The change in resonance frequencies of these eight lines upon rotating the crystal in 10° steps around two orthogonal axes is shown in Figures 2(b) and (c). These results can then be analysed to yield the principal values and orientations of both the ^{2}H CSA and quadrupolar tensors for both the amide and carboxyl hydrogens in NAV. As described in Ref. [11], it was found that, while the eigenvectors corresponding to the largest and intermediate principal values of the quadrupolar interaction are aligned (within the experimental error) with the NH bond direction and normal to the peptide plane, respectively, small but significant deviations are observed for the orientation of the CSA tensor.

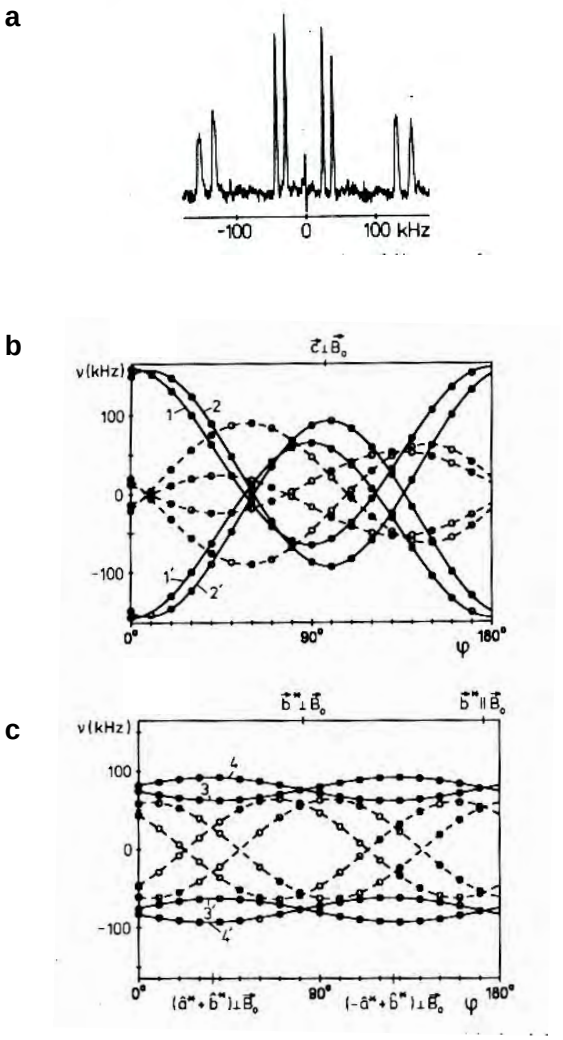

Figure 2. (a) ^{2}H NMR spectrum for a particular orientation of a single crystal of the peptide *N*-acetyl-D, L-valine (NAV) for which the exchangeable amide and carboxyl hydrogens were deuterated. (b), (c) The change in the resonance frequencies of the eight lines upon rotating the crystal in 10° steps around two orthogonal axes. (Reproduced by permission of the American Chemical Society from Ref. [11].)

Although the power of the single crystal method is evident, it suffers from a couple of significant limitations. Firstly, a single crystal of sufficient size, several mm in each dimension, with a typical volume of 50 mm^3, is necessary. Secondly, a specialised NMR probe incorporating a goniometer is required for the well-defined rotation of the sample, and such equipment is available in only a handful of laboratories worldwide. If, however, both the crystal and the equipment are available, this kind of study yields very precise measurements of parameters that are not available from diffraction techniques.

At this point, we mention a related class of sample, namely oriented samples. In the case of a perfect macroscopic ordering, each equivalent nucleus is oriented identically, and the situation is the same as that in a single crystal. Specific oriented samples of relevance (with varying degrees of ordering) include polymer fibres,[4] liquid crystals (LC),[12,13] and membrane proteins in oriented lipid bilayers[14]. We will return to the latter two cases in the discussion of two-dimensional experiments in sections 5 and 6.

2.3 Powder Spectra

In solid-state NMR, it is more usual to deal with a powdered sample, where there is a uniform distribution of molecular orientations over three-dimensional space. The NMR spectrum for a powdered sample, therefore, consists of a superposition of many lines, corresponding to all the possible resonance frequencies, where each line originates from a given nucleus in a particular crystallite. Examples of powder spectra are shown in Figures 3 and 4. In Figure 3, the anisotropic broadening is due to the CSA of a spin I = 1/2 nucleus, e.g. ^{13}C, (for three different values of the asymmetry parameter, δ (see Appendix)), while Figure 4 corresponds either to a dipolar coupling between an isolated pair of spin I =1/2 nuclei or to the first-order quadrupolar coupling of a spin I = 1 nucleus, e.g., ^2H.

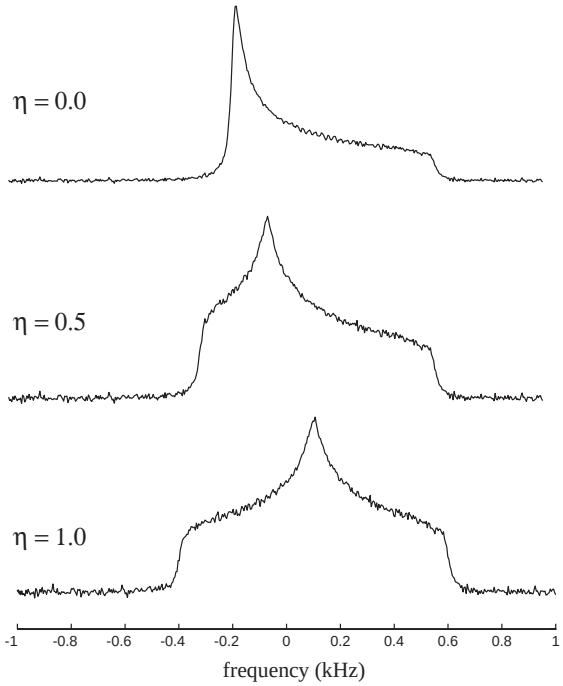

Figure 3. Simulated static powder spectra (with added noise) for the anisotropic broadening due to the CSA of a spin I = 1/2 nucleus, e.g. ^{13}C. Spectra are shown for three different values of the asymmetry parameter, δ (see Appendix). (Reproduced by permission of the Società Italiana di Fisica from Ref. [5].)

If powder spectra of the type shown in Figures 3 and 4 can be obtained experimentally, the principal values of the anisotropic interaction in question (though

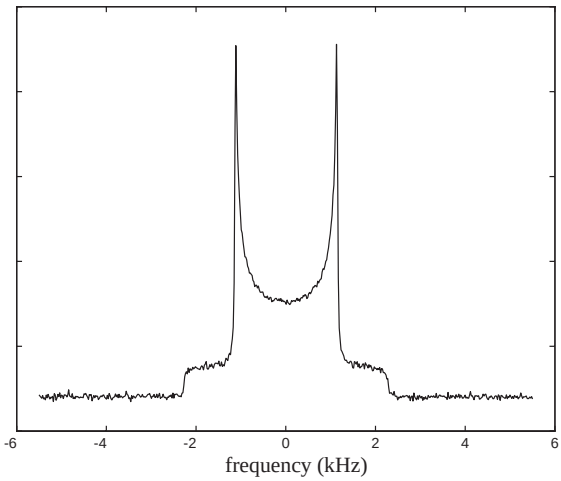

Figure 4. Simulated static powder spectrum (with added noise) for the anisotropic broadening due either to a dipolar coupling between an isolated pair of spin I =1/2 nuclei or to the first-order quadrupolar coupling of a spin I = 1 nucleus, e.g., ^{2}H. (Reproduced by permission of the Società Italiana di Fisica from Ref. 5.)

not the orientation of the PAS with respect to a fixed frame) can be obtained by a straight-forward lineshape analysis. However, to obtain such spectra, it is necessary that there is only one distinct nucleus, and that one anisotropic interaction dominates. Usually, the static NMR lineshape is a "broad featureless hump" due to the overlapping of many powder patterns as well as the interplay of the different broadening mechanisms. As an example of this, Figure 5 presents a ^{1}H NMR spectrum of a representative organic solid, together with, for comparison, the corresponding solution-state ^{1}H spectrum. It is to be noted that the problem in such a case is not a lack of information, but rather there is essentially an overload, such that the net effect is the virtual loss of all information. In the remainder of this article, solid-state NMR approaches by which this information can be recovered will be demonstrated.

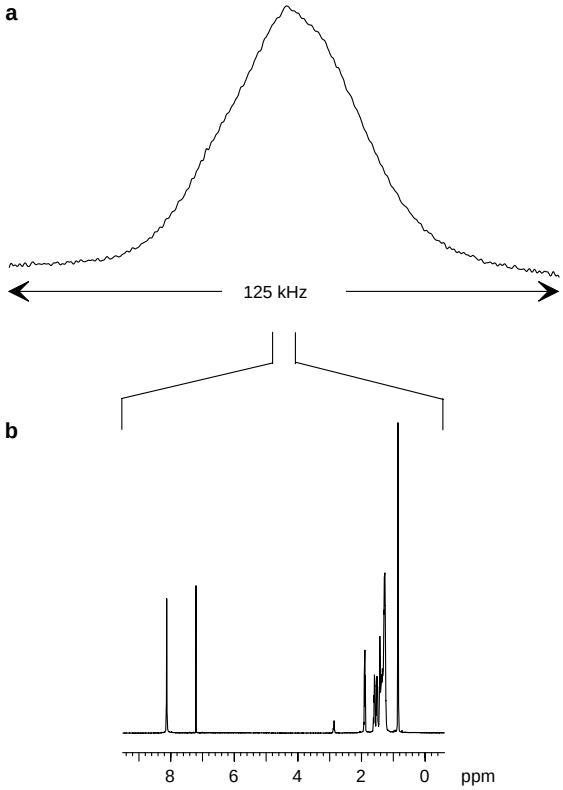

Figure 5. A comparison of the (a) static solid-state and (b) solution-state ^{1}H NMR spectra of a typical organic compound. (Reproduced by permission of the American Chemical Society from Ref. 7.)

2.4 One-dimensional ^{2}H NMR

One notable case where it is possible to obtain powder spectra due to a single resonance for the case where one broadening mechanism dominates is ^{2}H NMR. Since the natural abundance of deuterium is very low (see Table 1), the ^{2}H NMR spectrum of a sample which has been selectively deuterated at a particular hydrogen position contains, to an extremely good approximation, only the response of that particular ^{2}H nucleus. Moreover, ^{2}H is a spin I = 1 nucleus, and it, therefore, possesses a quadrupole moment. Although the ^{2}H quadrupolar coupling (~ 200 kHz) is relatively small as compared to other quadrupolar nuclei, it

still dominates the other anisotropic interactions in diamagnetic compounds, i.e., the CSA and the dipolar coupling.

The applications of ^{2}H NMR usually relate to the investigation of dynamic processes.[4] Indeed, one of the most important facets of solid-state NMR, in general, is its ability to probe molecular dynamics with atomic site selectively. This ability to probe dynamics is a direct consequence of the orientational dependence of the NMR resonance frequency: a given motional process leads to a particular crystallite experiencing a range of different orientations and hence a range of different frequencies. The motion is thus reflected in a marked change in the NMR spectrum as compared to the static case, with an extreme example of this phenomenon being the complete removal of anisotropic broadening as a consequence of isotropic molecular tumbling in solution. Notably, solid-state NMR spectra are not only sensitive to the *rates* of dynamic processes but also the *geometry*.

In ^{2}H NMR of a selectively labelled molecule, the one-dimensional (1D) powder spectrum depends only on the quadrupolar interaction for a single resonance. Moreover, the quadrupolar interaction for a deuteron bonded to a carbon atom is invariably axially symmetric and aligned with the bond direction. By recording a series of spectra at different temperatures, it is therefore possible, by means of a relatively straightforward lineshape analysis based on computer simulations, to determine the kinetic parameters, i.e., the rate constants and the activation energy, as well as the motional mechanism for the dynamic process under investigation. Moreover, such investigations are aided by the fact that the experiment can be performed over a very wide temperature range, since the sample is static and in the solid-state (i.e., there is no problem with a solvent freezing or evaporating). It should be noted that it is usual practice to record ^{2}H powder spectra using the quadrupolar (or solid) echo technique.[15]

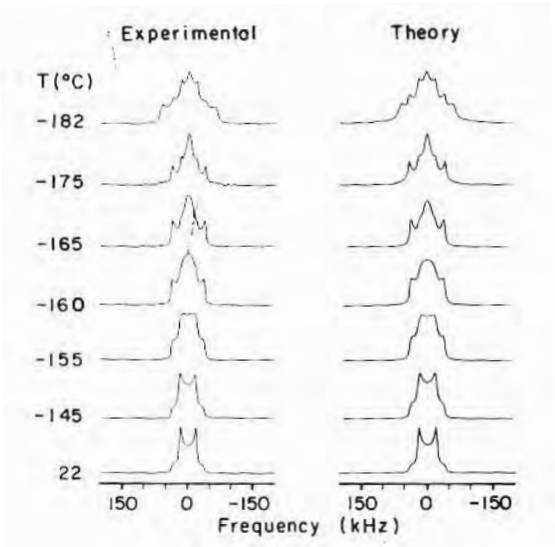

Figure 6. Variable-temperature ^{2}H NMR spectra recorded for a sample of [18-CD_3]-6-*s*-cis-retinoic acid. Best-fit spectra simulated for a model invoking a three-site jump motion are shown to the right of the corresponding experimental spectra. (Reproduced by permission of the American Chemical Society from Ref. 16.)

As a specific example, consider the ^{2}H NMR spectra shown in Figure 6, which were recorded for a sample of [18-CD_3]-6-*s*-cis-retinoic acid, such that the motion of the methyl hydrogens could be

investigated.[16] Marked changes in the spectra are apparent upon increasing the temperature. In particular, as well as changing its shape, the linewidth is observed to narrow by approximately a factor of two, when comparing the spectra for the lowest (top) and highest (bottom) temperatures. The rate constant for a model invoking a three-site jump motion was determined at each temperature by means of a lineshape analysis, and in Figure 6, the best-fit simulated spectra are shown to the right of the corresponding experimental spectra. For the lowest (top) and highest (bottom) temperatures investigated, the rate-constant was determined to be 2.3×10^4 and 1.5×10^{10} s^{-1}, respectively. These two temperatures, therefore, correspond to a motion which is, respectively, "slow" and "fast" compared to the relevant timescale of this NMR experiment (corresponding, in this case, to the time required to record the free-induction decay (FID)). From the knowledge of the rate constant for each temperature, it was possible to determine an activation energy of 14.5 $kJmol^{-1}$. By additionally investigating the methyl group jump motion in the corresponding trans model compound as well as in the membrane protein bacteriorhodopsin, Copié *et al* were able to postulate the existence of a 6-*s*-trans chromophore in the protein.[16]

3 MAGIC-ANGLE SPINNING

The above example of the effect of dynamics on a ^2H NMR powder spectrum illustrates that motion leads to line narrowing. Moreover, as noted above, in solution, fast isotropic tumbling of the molecules causes the averaging *to zero* of the line broadening due to the anisotropic interactions. To achieve high resolution, the solid-state NMR spectroscopist would like to mimic this averaging process. Rather than requiring random isotropic motion of each molecule, it can be shown that a physical rotation of the whole sample around an axis inclined at an angle of $\arctan(\sqrt{2}) = 54.7^o$ (referred to as the magic angle) to B_0 suffices to average any second-rank tensor interaction to zero.[17,18]

To understand why so-called magic-angle spinning (MAS) is so successful as a means of line narrowing, it is first necessary to recognise that the CSA, dipolar, and first-order quadrupolar interaction all have basically the same orientational dependence: for an axially symmetric tensor (this is always the case for the dipolar interaction, and corresponds to a CSA or first-order quadrupolar interaction with a zero asymmetry parameter), the orientationally dependent part of the frequency of a particular crystallite can be expressed in the form

$$\omega \propto 1/2\,(3\cos^2\theta - 1)\,, \qquad (1)$$

where θ denotes the angle between the tensor PAS direction and B_0 (see the Appendix for the full mathematical expressions). For a static sample, there is thus no anisotropic frequency shift for those crystallites with $\theta = 54.7^o$.

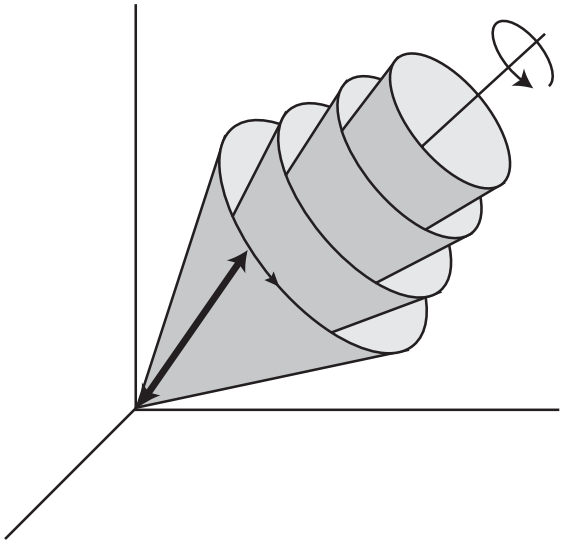

Figure 7. The effect of MAS for the specific example of a dipolar coupling between two spins. The four cones represent the range of positions adopted over the course of one rotor period for four different orientations of the internuclear vector relative to the rotor axis. The double-headed arrow represents an arbitrary position of one of the internuclear vectors.

To illustrate the effect of MAS, we consider in Figure 7 the specific example of a dipolar coupling between two spins. The four cones represent the range of positions adopted over the course of one rotor period for four different orientations of the internuclear vector relative to the rotor axis. In each case, the sample rotation leads to those components *perpendicular* to the rotation axis being zero on average, and only the component *parallel* to the rotation axis remains non-zero on average. Thus, for any original orientation, rotation around an axis yields an "average orientation" parallel to the axis of rotation. If the rotation axis is inclined at the magic angle to B_0, this parallel component has an anisotropic frequency shift equal to zero for all cases. Thus, under MAS, the anisotropic broadening is averaged to zero by the sample rotation for all crystallite orientations.

3.1 CP MAS NMR

For solid-state NMR of a dilute spin $I = 1/2$ nucleus, e.g. ^{13}C or ^{29}Si, MAS is usually combined with the method of cross polarisation (CP)[19,20], whereby a sensitivity enhancement results as a consequence of the transfer of polarisation from an abundant nucleus with a high magnetogyric ratio, usually ^{1}H – the approach is referred to as CP MAS NMR.[21] High-power proton decoupling is normally applied during the acquisition of the FID to remove broadenings due to dipolar couplings involving the protons, such that the dominant anisotropic broadening is the CSA.

The simulated spectra in Figure 8 illustrate the effect of MAS for the case of a CSA interaction. Upon rotating the sample, the static lineshape is seen to break up into a centreband and spinning sidebands, separated by the rotor frequency. At a low MAS frequency, ν_R, the sideband manifold is observed to map out the shape of the static pattern. As the ν_R is increased, the signal intensity is increasingly concentrated at the centreband position, which corresponds to the isotropic chemical shift. It is to be noted that the linewidths are narrow and independent of ν_R.[22]

In principle, it is possible to extract the anisotropy and asymmetry of the CSA

by fitting the observed MAS sideband intensities. This is referred to as a Herzfeld-Berger analysis.[23] Such an approach is restricted to relatively small molecules, since it is necessary to be able to resolve, at a low ν_R, the sidebands of different resonances. As the number of distinct resonances increases, the 1D spectrum becomes increasingly more crowded; the advantage of extending the experiment to a second dimension in such cases will be discussed in section 5.

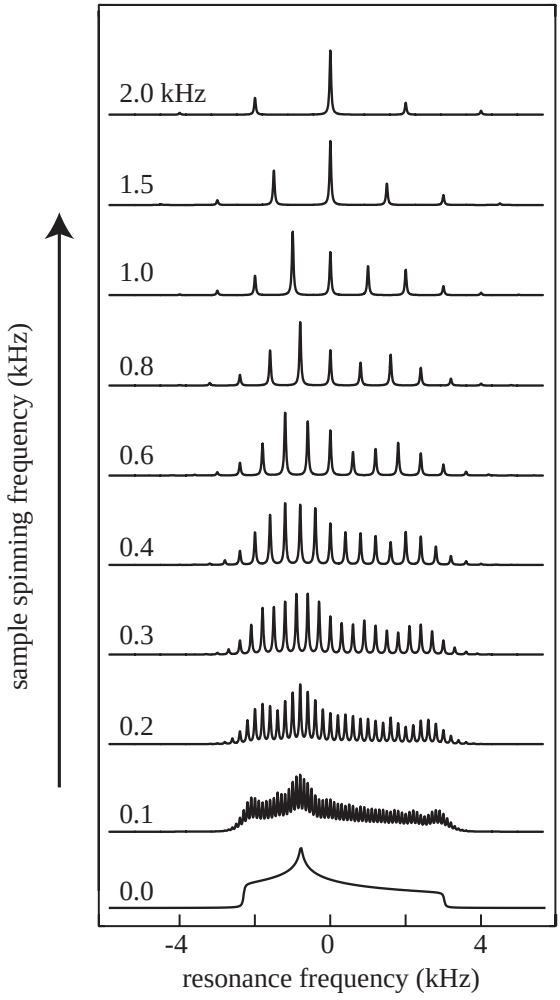

Figure 8. Simulated spectra showing the effect of MAS on the anisotropic lineshape due to a CSA interaction. (Reproduced by permission of the American Institute of Physics from Ref. [24].)

The main interest of the CP MAS technique is that it can provide high-resolution purely isotropic spectra. As is apparent from Figure 8, as ν_R is increased such that it becomes large as compared to the static linewidth, the signal is increasingly concentrated in the centreband position. The spectrum is obviously much simplified if there is only one narrow resonance line, at the isotropic chemical shift, for each distinct nucleus. As an example, Figure 9 presents a ^{13}C CP MAS spectrum of powdered cyclosporin A, a cyclic 11-residue peptide. In this case, the isotropic spectrum is obtained by employing a ν_R of 33.3 kHz, and there are virtually no spinning sidebands. (MAS probes capable of supporting such a ν_R have only become available in the last 2-3 years. It is to be noted that at such a fast ν_R, it is necessary to employ a modified CP procedure, which is referred to as ramped CP.[25,26]) An alternative means by which a purely isotropic spectrum without spinning sidebands can be achieved for the case of a moderate ν_R is to employ a specially designed sequence of radiofrequency (*rf*) pulses to suppress the spinning sidebands – the classic example is the TOSS (total suppression of sidebands) sequence,[27,28] which involves the application of four (or $2n + 2$) appropriately spaced 180° pulses before the start of acquisition.

In solid-state NMR experiments, a central theme is that of resolution. For ^{13}C CP MAS NMR, a critical factor in this respect is the efficiency of ^{1}H decoupling.

The simplest method, which is termed continuous wave (CW) decoupling, involves the application of a continuous *rf* pulse of fixed phase for the duration of the acquisition of the FID.[29] Recently, more sophisticated decoupling methods, such as TPPM[30] or other sequences possessing a RN_n^v symmetry,[31] have been introduced – an explanation of why these methods yield narrower ^{13}C linewidths than conventional CW decoupling is given in Refs. [31,32]. In simple terms, the efficiency of ^1H decoupling increases as the *rf* field strength increases (note that NMR literature usually refers to the inherent nutation frequency of the pulse, $|\omega_1| = |\gamma B_1|$, where B_1 is the *rf* field strength). Experimentally, care must of course be taken to find the power level which gives the optimum decoupling performance without damaging the probe. In Figure 9, it is shown that current state-of-the-art ^1H decoupling, namely TPPM at a ω_1 of 200 kHz, yields a ^{13}C linewidth (full-width at half-maximum height, FWHMH) of 14 Hz (see the inset for a methyl carbon in cyclosporin A). The spectrum in Figure 9 was recorded at a B_0 of 11.8 Tesla (corresponding to ^1H and ^{13}C Larmor frequencies of 500 and 125 MHz). Today, solid-state NMR is being performed at B_0 fields approaching 20 Tesla; provided that the same or narrower linewidths (in Hz) can be achieved at the higher B_0, and this can certainly not be taken for granted in solid-state NMR, the resolution of resonances with different chemical shifts will be further improved at higher B_0.

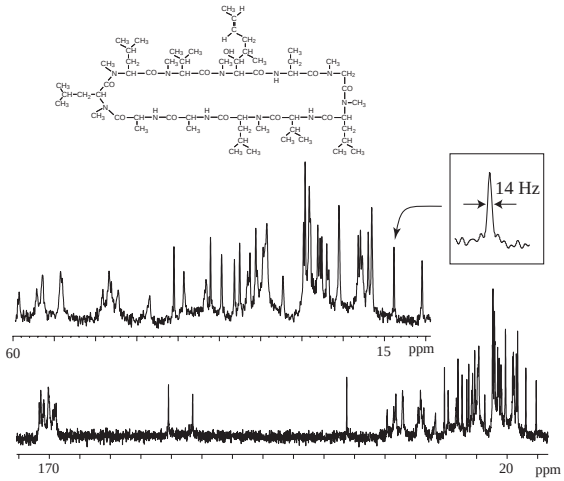

Figure 9. A ^{13}C CP MAS (ν_R = 33.3 kHz) spectrum of powdered cyclosporin A, a cyclic 11-residue peptide, at natural abundance. (Courtesy of A. Lesage and P. Charmont.)

For small molecules, some of the ^{13}C resonances can usually be assigned by reference to an assigned solution-state spectrum, since ^{13}C chemical shifts are relatively insensitive to the through-space effects of importance in the solid phase. As the molecular size increases, however, this is no longer the case. To assign a complicated ^{13}C CP MAS spectrum, such as that in Figure 9, spectral editing methods which can distinguish between CH_3, CH_2, CH, and quaternary carbons are of much help.[33-36] As a specific example, Figure 10 shows a 1D ^{13}C spectrum of L-histidine monohydrochloride monohydrate recorded using the SS-APT (solid-state attached proton test) method:[34] resonances due to carbons with an even (i.e., quaternary and CH_2 moieties) or odd (i.e., CH and CH_3 moieties) number of attached protons are positive or negative, respectively. It is to be noted that the SS-APT method is based on through-bond *J* couplings, and thus has the advantage of being unaffected by molecular motion,

which can lead to the erroneous interpretation of spectra obtained with the other spectral editing methods which exploit through-space dipolar couplings.

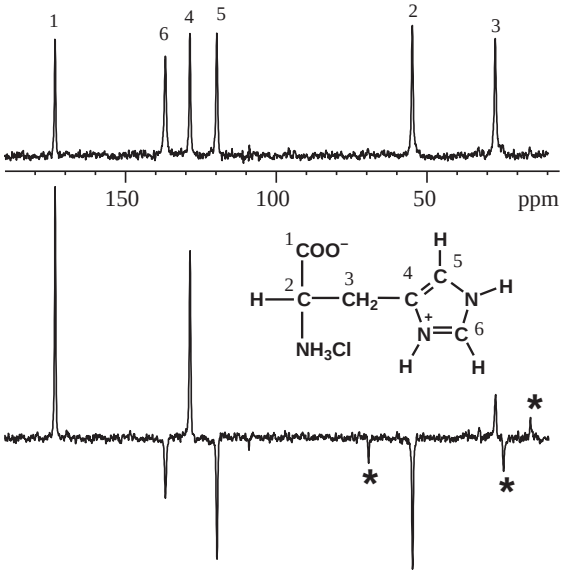

Figure 10. 1D ^{13}C spectrum of L-histidine monohydrochloride monohydrate recorded using the SS-APT method. Resonances due to carbons with an even (i.e., quaternary and CH_2 moieties) or odd (i.e., CH and CH_3 moieties) number of attached protons are positive or negative, respectively. Spinning sidebands are labelled by asterisks. For comparison, the ^{13}C CP MAS spectrum is shown at the top. (Reproduced by permission of the American Chemical Society from Ref. 34.)

1D CP MAS is the workhorse solid-state NMR experiment, a fact which is apparent from the very wide range of applications, with specific examples including fossil fuels,[37] i.e., coals[38] and cokes[39], food science, e.g. polysaccharides,[40] pharmaceuticals,[41] polymer blends[42] and soil science[43]. In addition to ^{13}C and, to a lesser extent, ^{15}N, another much investigated nucleus is ^{29}Si, with ^{29}Si solid-state NMR being of much importance in materials science and geology.[44,45] Although ^{31}P has a 100 % natural abundance, the relatively large separation between phosphorous atoms in a typical solid means that ^{31}P often has the characteristics of a rare spin. ^{31}P CP MAS NMR is of importance in, e.g., the investigation of glasses.[46]

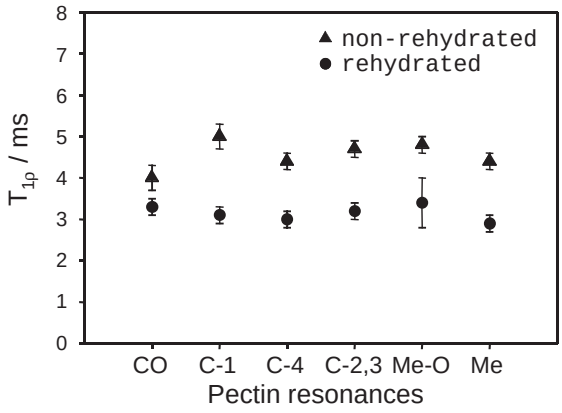

Figure 11. Fitted ^1H $T_{1\rho}$ relaxation time constants as read out at the various assigned ^{13}C resonances for 10 % hydrated (triangles) and 35 % hydrated (circles) onion cell-wall material. The difference directly reflects the increased mobility in the hydrated sample. (Reproduced by permission of Elsevier Science Publishers from Ref. 47.)

Valuable information can often be obtained by simple experiments which determine the relaxation times, in particular the spin-lattice (or longitudinal) relaxation times in the laboratory or rotating frame, namely the ^{13}C T_1 and the ^1H $T_{1\rho}$, respectively, for the different resolved resonances in a 1D CP MAS spectrum. In simple terms, a faster relaxation time is due to an increase in molecular mobility. As a specific example, Figure 11 shows the ^1H $T_{1\rho}$ relaxation time constants, as read out at the ^{13}C resonances, for the pectin resonances in onion cell-wall material.[47] It is apparent that increasing the sample hydration from 10 to 35 % leads to a clearly faster relaxation.

3.2 ^{1}H Solid-State NMR

In the discussion of Figure 8, it was noted that the linewidths of the centreband and spinning sidebands are narrow and independent of ν_R. This is a general feature of *rare spin* spectra. A different situation is usually encountered in ^{1}H solid-state NMR: Figure 12 shows the effect of increasing ν_R upon the centreband in the ^{1}H MAS NMR spectrum of a medium-sized organic solid. In particular, it is apparent that the linewidth is dependent on ν_R, with a line narrowing being observed upon increasing ν_R. Even at 35 kHz, the linewidths (FWHMH ≈ 750 Hz) are, however, much larger than those observed in ^{13}C MAS spectra.

The different effect of MAS in ^{1}H and ^{13}C NMR is a consequence of the central importance and relative insignificance of homonuclear (i.e., between like spins) dipolar couplings in the respective two cases. The homonuclear dipolar coupling between a pair of protons is approximately 16 times larger than that between two ^{13}C nuclei at the same internuclear separation. Moreover, the natural abundance of ^{13}C is only 1 % as opposed to nearly 100 % for ^{1}H, such that (except for the case of isotopically enriched samples) very few ^{13}C nuclei have a nearby ^{13}C neighbour.

For a typical organic solid, there exists a strongly dipolar-coupled multi-proton network, and the effect of MAS is quite different as compared to the case of the CSA interaction. This difference is explained in a classic paper by Maricq and Waugh.[22] The CSA is an example of an interaction where the anisotropic broadening is perfectly refocused at the end of each rotor period, τ_R, (in the language of quantum mechanics, the corresponding Hamiltonian for a given crystallite commutes with itself at all times). By comparison, when there are three or more dipolar-coupled protons, the perturbing influence of the other dipolar-

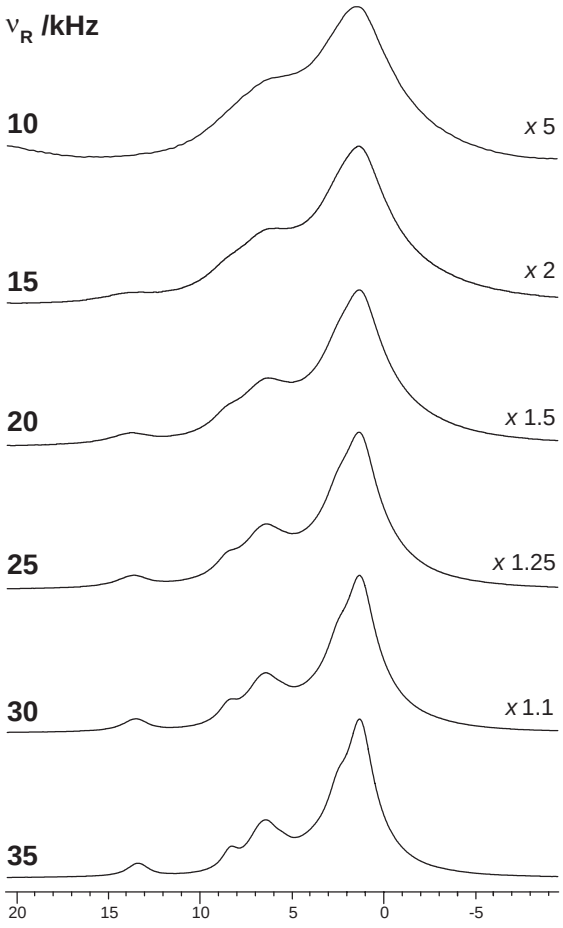

Figure 12. The effect of increasing the MAS frequency, ν_R, on the centreband of a ^{1}H MAS spectrum of a typical organic compound. (Reproduced by permission of the American Chemical Society from Ref. [48].)

coupled protons upon a particular dipolar-coupled pair means that the Hamiltonian does not commute with itself at all times, and the evolution under the dipolar coupling of a particular pair is no longer refocused at the end of each τ_R.

It was noted in the previous section, that a ν_R in excess of 20 kHz has only become possible in the last 2-3 years. The advantage in terms of the enhanced line narrowing in a ^{1}H MAS NMR spectrum is evident in Figure 12. Indeed, it has been shown that a ν_R of 30+ kHz at a ^{1}H Larmor frequency of 500+ MHz is sufficient to allow some ^{1}H resonances due to particular chemically distinct protons to be resolved in ^{1}H MAS NMR spectra of small to moderately sized organic solids.[48-51] The line narrowing achieved by MAS alone at a ν_R equal to 30 kHz is, however, still far from the limiting case, where all residual dipolar broadening has been removed.

Brute-force fast MAS is not the only means by which line narrowing can be achieved in solid-state NMR. A particularly ingenious alternative approach, first presented over 30 years ago by Waugh and co-workers, involves the removal of the dipolar broadening by specific multiple-pulse techniques, where radiofrequency (rf) pulses achieve rotations in spin space.[52,53] These rotations can complement the effect of the physical rotation of the sample; combined rotation and multiple-pulse spectroscopy (CRAMPS)[54-56] yields well-resolved ^{1}H spectra.[57] We will discuss the CRAMPS approach in more detail in section 5.3.

An inspection of Table 1 reveals that ^{19}F has similar NMR properties to ^{1}H. Thus, methods which deal with the residual broadening due to homonuclear dipolar couplings are also of much relevance in ^{19}F solid-state NMR.[58] Although fluorine is much less commonly encountered in chemistry than the omnipresent hydrogen, ^{19}F solid-state NMR has found a number of important applications, with recent examples including fluoropolymers[59] and biomembranes[60].

4. RECOUPLING METHODS

Anisotropic interactions present both problems and opportunities. On the one hand, there is the significant disadvantage of hindering the resolution of distinct sites, and methods, such as MAS, which remove the line broadening due to the anisotropic interactions are essential to allow the recovery of the isotropic chemical shift information. On the other hand, they contain valuable structural and dynamic information. This information can be accessed while maintaining high resolution by employing a so-called recoupling method[8,9] to recover the anisotropic interaction during part of the NMR experiment. In simple terms, recoupling involves the application of *rf* pulses to counteract the effect of the physical rotation. The conceptually most

simple technique to illustrate the principle is REDOR.

4.1 Heteronuclear Dipolar-Coupled Spins: REDOR

In the rotational-echo double-resonance (REDOR)[61-63] technique, the distance between two heteronuclei is determined by comparing the signal intensity in two closely related experiments. The interpretation of the experimental results assumes the existence of isolated spin pairs, and there is thus usually a requirement for selective isotopic labelling at the two sites, the distance between which is of interest.

In a reference experiment, an echo corresponding to the refocusing of the evolution under both the chemical shift and the heteronuclear dipolar coupling is formed. The echo intensity in the reference experiment, S_0, is then compared to that in a second experiment where the application of 180° pulses at intervals of $\tau_R/2$ on the channel where there is no transverse magnetisation interferes with the refocusing by MAS of the evolution due to the heteronuclear dipolar coupling, and hence results in a reduced signal intensity, S_r. For an isolated spin pair, the ratio S_r/S_0 depends solely and in a straightforward manner on the product of the evolution time and the heteronuclear dipolar coupling. The REDOR master curve applicable to all heteronuclear spin pairs is plotted in Figure 13. Note that it is common to see the REDOR literature referring to the difference, $\Delta S = S_0 - S_r$. By simple reference to this master curve, it is possible to determine the heteronuclear dipolar coupling between the spin pair under consideration. It is of course advisable to determine two or more S_r values to ensure the reliability of the analysis. Since the dipolar coupling depends on the internuclear distance to the inverse cubed power (see Appendix), this method allows the determination of internuclear distances for heteronuclear spin pairs.

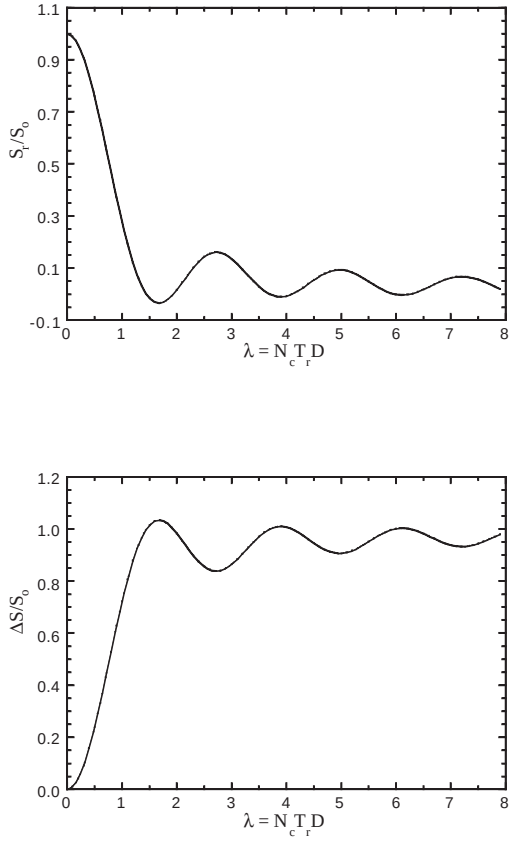

Figure 13. REDOR master curves for an isolated dipolar-coupled spin pair showing the dependence of the ratios S_r/S_0 and $\Delta S/S_0$ upon the product of the evolution time and the heteronuclear dipolar coupling. (Reproduced from Ref. 63.)

A number of interesting applications of the REDOR method have

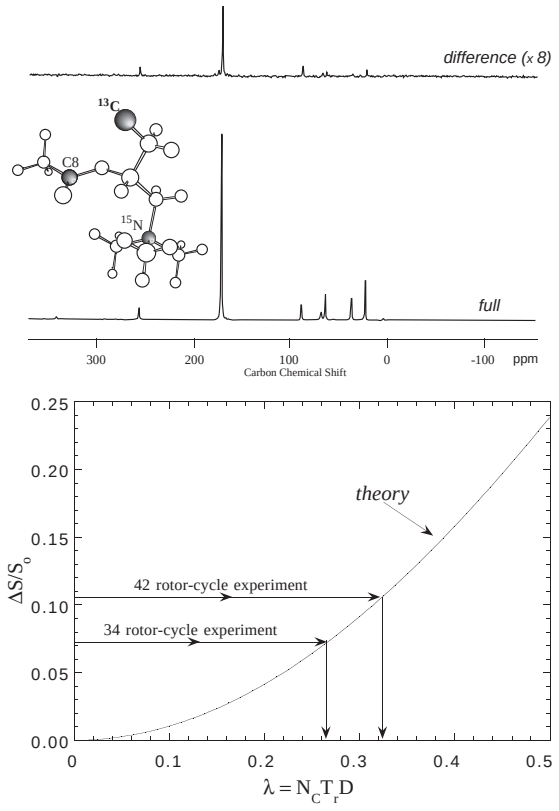

Figure 14. The determination of the distance between the specific spin labels in [1-^{13}C, ^{15}N]acetyl-L-carnitine by the REDOR technique. The difference, ΔS, and reference, S_0, REDOR spectra are shown for the 34-τ_R experiment. (Reproduced from Ref. 63.)

been presented (see Table 1 of Ref.9), with a particular emphasis on samples of biological relevance. A specific example is shown in Figure 14, where the distance between the specific spin labels in [1-^{13}C, ^{15}N]acetyl-L-carnitine is determined to be 0.496 nm.[63] In this particular case, a distance determination was possible even though the C1 resonance is not resolved from that of the indicated C8 carbon. As well as ^{13}C and ^{15}N, other spin I = 1/2 nuclei studied by REDOR include ^{19}F, ^{29}Si, and ^{31}P. For example, Holl *et al* have demonstrated the measurement of an 0.8 nm ^{13}C-^{19}F internuclear distance in a nine-residue fragment of the peptide antibiotic emerimicin.[64] Extensions of the REDOR method to measure distances where one or even both of the nuclei are quadrupolar have also been proposed. For quadrupolar nuclei, the large quadrupolar interactions presents significant problems, in particular a simple 180° pulse does not achieve a uniform inversion for all crystallites for the case of a broad quadrupolar lineshape. Various methods, e.g. TRAPDOR[65] and REAPDOR[66], have been introduced which attempt to address this problem.

4.2 Homonuclear Dipolar-Coupled Spins

There are small but important differences between the evolution of a given spin under a homonuclear as opposed to a heteronuclear dipolar coupling.[3-5] As a consequence, a different methodology is required for the determination of the internuclear distance between a homonuclear dipolar-coupled pair of spins.

Rotational resonance (RR) is an intriguing phenomenon which is observed when ν_R is equal to a small integer multiple of the difference in the isotropic chemical shift frequencies of two resonances in the spectrum.[67,68] The most apparent effect of RR is that the normally narrow spectral peaks acquire splittings and broadenings, the nature of which depend on the dipolar coupling between the two spins. As a specific example, experimental spectra (together with best-fit simulations) corresponding to the n = 1, 2,

and 3 RR conditions for all-*E*-[11,20-$^{13}C_2$]-retinal are shown in Figure 15.[69] In this case, it was possible to determine that the internuclear distance between the two ^{13}C labels is 0.301 ± 0.008 nm.

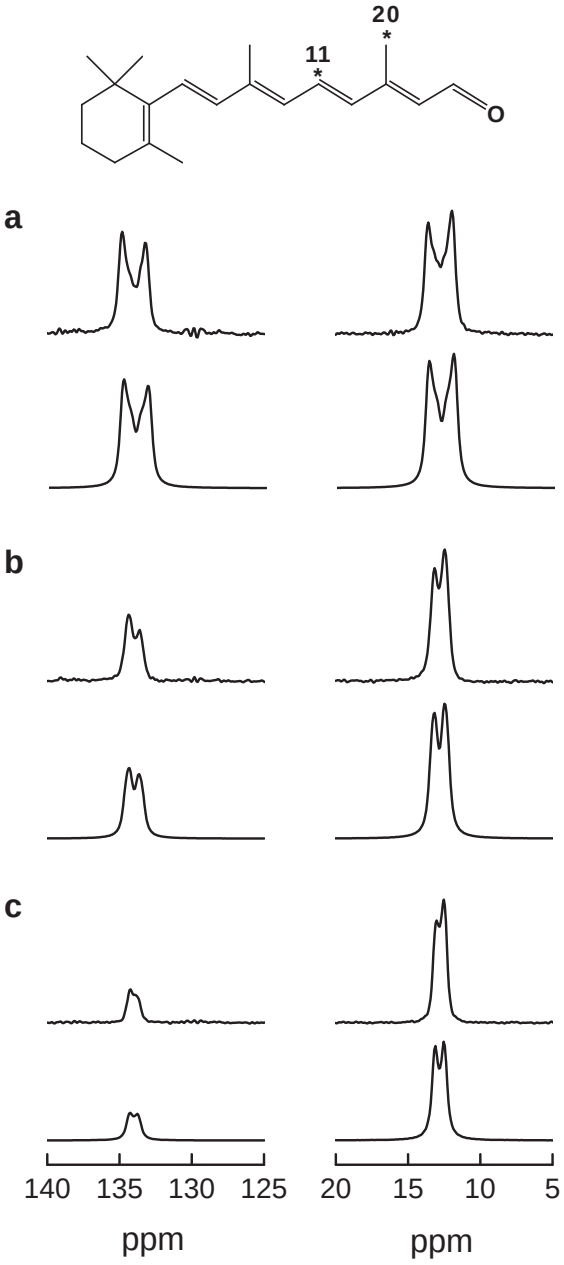

Figure 15. ^{13}C rotational-resonance experimental spectra (top), together with best-fit simulations (bottom), corresponding to the n = (a) 1, (b) 2, and (c) 3 RR conditions for all-*E*-[11,20-$^{13}C_2$]-retinal. (Reproduced by permission of Elsevier Science Publishers from Ref. [69].)

In the last decade, a large number of methods for recoupling the homonuclear dipolar coupling have been developed, with specific examples including DRAMA,[70] RFDR,[71] HORROR[72], C7,[73] BABA,[74] DRAWS[75] and DREAM[76] (for a comprehensive account see Refs.[8,9]). We note that Levitt and coworkers have recently introduced a very helpful classification system, based on symmetry principles, which explains how many of these sequences work and provides a framework for generating other sequences.[31,77] Rather than allowing the accurate determination of internuclear distances, these sequences, as will be illustrated in section 5, are usually employed to establish correlations or to select dipolar-coupled spin pairs in multi-dimensional homonuclear experiments.

4.3 The CSA: CODEX

It was stated above that MAS causes the evolution under the CSA to be refocused at the end of each τ_R. If a 180° pulse is applied every $\tau_R/2$, the refocusing of the CSA evolution is prevented (the same principle applies for the case of the heteronuclear dipolar coupling in the REDOR experiment (see section 4.1) or the homonuclear dipolar coupling in the RFDR[71] sequence). Recently, deAzevedo *et al* have shown how an experiment incorporating two periods of such CSA recoupling separated by a mixing time, τ_m, allows the detection of slow dynamic processes.[78,79] The method is applicable at fast MAS, and is termed centreband-

only detection of exchange (CODEX). The principle of the experiment is that a loss of signal intensity is observed if the orientation of the CSA tensor for a particular carbon changes during τ_m. By subtracting the signal intensity from that measured in a reference experiment, a pure-exchange CODEX spectrum is obtained.

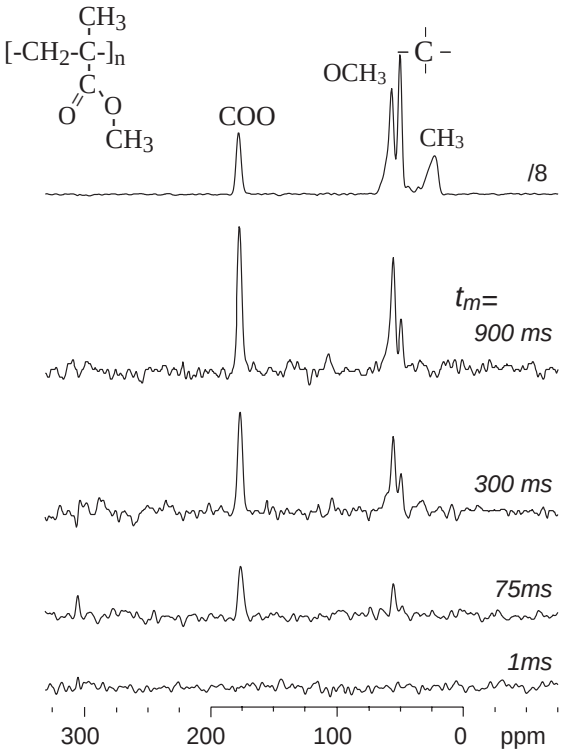

Figure 16. Pure-exchange CODEX ^{13}C NMR spectra, recorded for a sample of amorphous PMMA, (at natural abundance in ^{13}C) at 300 K with different τ_m. A ^{13}C CP MAS spectrum is shown at the top. (Reproduced by permission of the American Chemical Society from Ref. 78.)

As a specific example, Figure 16 shows pure-exchange CODEX ^{13}C NMR spectra, recorded for a sample of amorphous poly(methyl methacrylate), PMMA, (at natural abundance in ^{13}C) at 300 K with different τ_m.[78] For the very small mixing time, τ_m, of 1 ms, no intensity is observed, indicating the absence of dynamics on this timescale. For a longer τ_m, intensity is seen to build up at the COO and OCH_3 positions as well at the quaternary C position due to side group and backbone motion, respectively, in the polymer. From a series of CODEX experiments, it is possible to determine the reorientation angle, the correlation time, as well as the fraction of mobile segments.

5 HOMONUCLEAR TWO-DIMENSIONAL EXPERIMENTS

The importance of solution-state NMR today owes much to the extension of the experiment to a second (and higher) dimension.[1] Two-dimensional (2D) NMR spectroscopy is also of much significance in solid-state NMR. In attempting to classify the many important different 2D solid-state NMR experiments which have been proposed to date, we make, in this article, a distinction between homonuclear (i.e., those involving only one kind of nucleus) and heteronuclear experiments.

5.1 Establishing The Backbone Connectivity in an Organic Molecule

In Section 3.1, the problem of assigning the many resolved ^{13}C resonances in a 1D MAS spectrum was mentioned, and 1D spectral editing methods were introduced. In this section, we describe homonuclear ^{13}C-^{13}C 2D correlation experiments in which a selection is usually made such that 2D peaks are only observed for pairs of directly-bonded carbons (or at least these

peaks are significantly more intense). In this way, it is possible to trace out the connectivity along the backbone of the organic molecule, and thus assign the ^{13}C resonances. As a consequence of the significant sensitivity problems associated with the very low probability of finding a pair of directly bonded ^{13}C nuclei in a sample at natural abundance, these experiments are usually performed on fully or partially ^{13}C enriched (normally globally, i.e. at all carbon positions) samples.

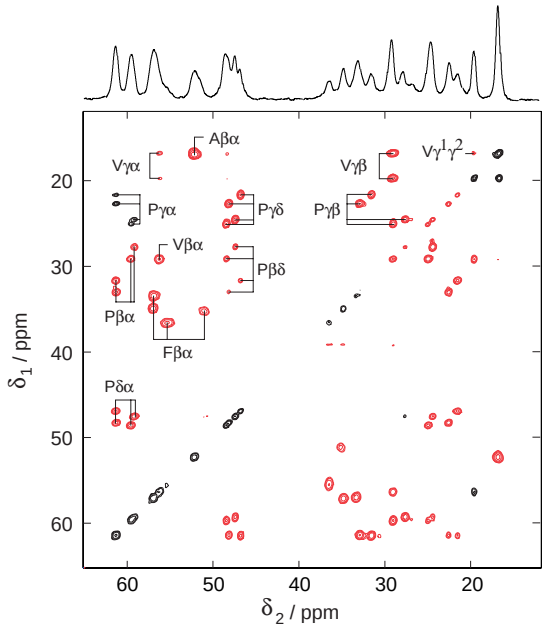

Figure 17. The region corresponding to the C_α and aliphatic side-chain carbons of a ^{13}C-^{13}C SQ-SQ correlation spectrum of ^{13}C globally-labelled antanamide (Val-Pro-Pro-Ala-Phe-Phe-Pro-Pro-Phe-Phe), recorded at a magnetic field of 14.1 T and a ν_R = 30 kHz. Mixing was achieved using a DREAM[76] recoupling sequence of duration 7 ms. Positive and negative peaks are shown as dark- and light-shaded lines, respectively. The indicated negative off-diagonal peaks are due to one-bond correlations among the aliphatic side-chains. (Courtesy of B. H. Meier.)

In the first class of ^{13}C-^{13}C 2D correlation experiments described here, SQ coherence (SQC), i.e., that which is detected in a conventional 1D NMR experiment, evolves in both dimensions of the NMR experiment. A mixing time is inserted between the two evolution periods during which a pulse sequence is applied which recouples the homonuclear dipolar coupling (see section 4.2), such that coherence transfer occurs between ^{13}C nuclei which are close together in space. As a specific example, Figure 17 shows the region corresponding to the C_α and aliphatic side-chain carbons of a ^{13}C-^{13}C SQ-SQ correlation spectrum of ^{13}C globally-labelled antanamide (a cyclic decapeptide), recorded using the DREAM[76] recoupling sequence. The indicated negative off-diagonal peaks are due to one-bond correlations among the aliphatic side-chains.

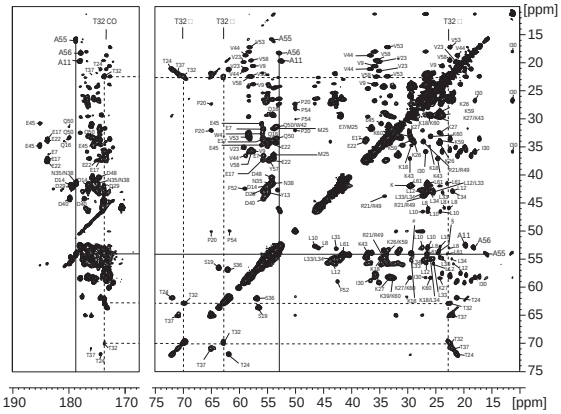

Figure 18. A 2D ^{13}C-^{13}C SQ-SQ correlation spectrum of a solid 62 residue ^{13}C and ^{15}N globally-labelled protein containing the α-spectrin SH3 domain, recorded at 17.6 T. Mixing was achieved using proton-driven spin diffusion; a long mixing time of 15 ms was employed such that longer-range correlations are also observed. (Reproduced from Ref. [80].)

By using very-high magnetic fields, ever larger biopolymers are becoming

accessible to solid-state NMR. As an example, Figure 18 presents a ^{13}C-^{13}C SQ-SQ correlation spectrum of a solid 62 residue ^{13}C and ^{15}N globally-labelled protein containing the α-spectrin SH3 domain, recorded at 17.6 T.[80] In this case, mixing was achieved using proton-driven spin diffusion; a long mixing time of 15 ms was employed such that longer-range correlations are also observed. Using this and other experiments, it was possible to assign all the ^{13}C and ^{15}N resonances.

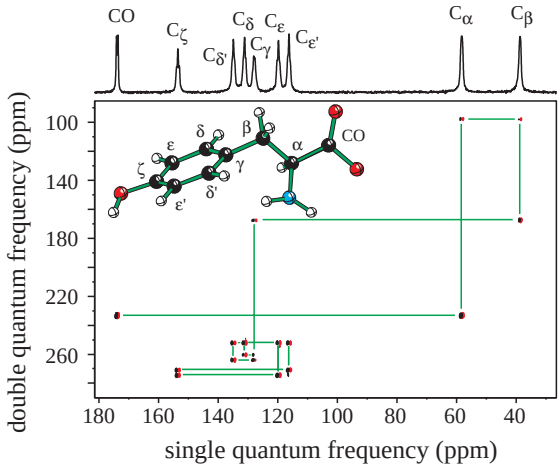

Figure 19. A 2D ^{13}C-^{13}C INADEQUATE spectrum of L-tyrosine.

Emsley and co-workers have recently suggested an alternative approach for establishing carbon-carbon connectivities, namely the solid-state INADEQUATE experiment.[81] It is so termed because of the analogy to the solution-state experiment of the same name.[82] Unlike the experiments described above which utilise through-space dipolar couplings, this approach is based on the through-bond *J* coupling. A further important difference is that double-quantum (DQ) coherence (DQC) as opposed to SQC evolves during the t_1 (or indirect) dimension of the experiment. Experiments involving the creation of DQC and multiple-quantum coherence (MQC) in general are of much importance in both solution-state and solid state NMR. For example, in pioneering work, Pines and co-workers have shown that the analysis by so-called spin-counting experiments of the very high MQC orders excitable in static ^{1}H solid-state NMR provides valuable information about large clusters (often up to 100 nuclei) of dipolar-coupled protons.[83,84]

For a detailed discussion of the concept of MQC, the reader is referred to e.g., Refs. [1,85]. Here, we simply note two relevant features: firstly, a MQC cannot be directly detected in an NMR experiment, i.e., an experiment involving a MQ evolution period is inherently at least 2D, since the MQC must be converted into detectable SQC; and, secondly, for spin I=1/2 nuclei, MQC can only be created for coupled nuclei. As illustrated by the specific example of L-tyrosine in Figure 19, an advantage over the SQ-SQ correlation spectra in Figures 17 and 18 is the absence of signal along the diagonal. Furthermore, by using the *J* coupling, the observation of a pair of correlated peaks can only be due to directly-bonded ^{13}C nuclei. However, the signal-to-noise ratio (S/N) of the *J*-coupled INADEQUATE experiment is invariably worse than that of the dipolar-based experiments used for Figures 17 and 18, although refocused INADEQUATE experiments[86,87] reduce

the signal loss and are applicable to disordered systems.

5.2 Dipolar-Mediated Double-Quantum Spectroscopy

DQ spectroscopy is not only useful for homonuclear ^{13}C-^{13}C correlation experiments which allow the identification of the backbone connectivity. In this section, the utility of other 2D DQ experiments which provide insight into, e.g., through-space proximities will be illustrated. As opposed to the solid-state INADEQUATE experiment introduced in the previous section, the experiments described in this section are based on the dipolar as opposed to the *J* coupling of spins.

A ^{1}H 2D DQ MAS spectrum[88] recorded in a rotor-synchronised fashion in t_1 (i.e., the t_1 increment is set equal to one rotor period such that all spinning sidebands in the DQ dimension (F_1) fold back onto the centreband position) is shown in Figure 20a. To create DQC as well as to allow its conversion into observable SQC, the BABA[74] recoupling sequence (see Section 4.2) was used – this is a robust sequence which is suitable for the fast ν_R of 35 kHz employed. The ability of the ^{1}H DQ MAS experiment to identify proton-proton proximities lies in the fact that both the excitation and subsequent reconversion of DQC relies on the presence of a dipolar coupling between a particular two spins. Since the dipolar coupling is proportional to the internuclear distance to the inverse cubed power, a peak is, hence, only observed in the DQ MAS spectrum if the corresponding two protons are close together in space. As a rule of thumb, the presence of a peak in a ^{1}H DQ MAS spectrum implies a proton-proton proximity of under 0.35 nm.

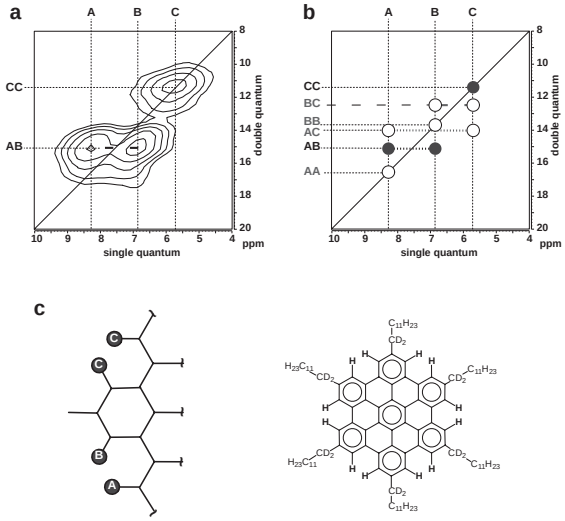

Figure 20. (a) A representative rotor-synchronised ^{1}H DQ MAS spectrum, corresponding to the aromatic protons in HBC-C_{12}. (b) A schematic representation showing the positions of the six possible DQ peaks; the observed AB and CC peaks (filled circles) imply the proton-proton proximities indicated in (c). (Reproduced by permission of Elsevier Science Publishers from Ref. [50].)

For this particular example, which corresponds to the aromatic protons of an alkyl-substituted polycyclic aromatic system (HBC-C_{12}),[49] three resonances (labelled A, B, and C) can be identified in the corresponding 1D ^{1}H (500 MHz) MAS spectrum, which is shown at the top of Figure 20a. The six possible DQ peaks in this case are shown in Figure 20b. Since the DQ frequency corresponding to a given DQC is simply the sum of the two SQ frequencies, DQCs between like (AA) and unlike (AB) spins can, in general, be

distinguished in that, in the former case, a single peak at ($2\nu_A$,ν_A) is observed, while, in the latter case, two peaks at (ν_A + ν_B,ν_A) and (ν_A + ν_B,ν_B) are observed. (The notation (ν_1,ν_2) refers to a DQ peak centred at ν_1 and ν_2 in the F_1 and F_2 dimensions, respectively.) Note that for the anisotropic dipolar coupling, it is, unlike for the isotropic *J* coupling, possible to observe an auto peak for a DQC between two like spins. It should be noted that an advantage of the DQ approach over a spin diffusion experiment[4,89] in which a mixing time is inserted between two SQ evolution periods is that an auto peak is only observed if there is a close proximity of two protons. By contrast, in the spin diffusion experiment, strong auto peaks are seen for all resonances regardless of whether there is a close proximity.

Of the six possible DQ peaks, only two, namely AB and CC, are observed in the experimental spectrum in Figure 20a. For this system, the aromatic protons are arranged into well-isolated pairs of 'bay protons'; the observed DQ peaks thus correspond to these bay protons pairs. As discussed in Ref. [49], the implied presence of only two types of pairs of aromatic protons, H_A-H_B and H_C-H_C (see Figure 20c) is a consequence of intermolecular ring current effects; for an isolated molecule, the six-fold symmetry leads to all aromatic protons being equivalent. Using quantum-chemical calculations of ^{1}H chemical shifts, the experimental data could be assigned in a fully quantitative manner to a particular structural model.[90] Such effects of ring currents on NMR chemical shifts are, of course, well established;[91] however, it is only recently, with the development of solid-state NMR methods allowing the resolution of ^{1}H resonances, that the widespread importance of these effects in organic solids is gaining attention; other clear examples of the phenomenon can be found in, e.g. Refs. [92,93]. It is to be noted that, although the absolute shifts due to ring currents are similar for both ^{1}H and ^{13}C, the much smaller range of chemical shifts (~20 ppm as opposed to 200 ppm) means that the influence is much more evident in ^{1}H NMR. In addition, protons are normally located at the more exposed parts of the structure.

^{1}H NMR is well suited for the investigation of hydrogen bonding, with it being well known that hydrogen bonding leads to a marked lowfield (to a high ppm value) chemical shift. For example, for a general hydrogen bond O–H···O, a clear correlation between the ^{1}H isotropic chemical shift and the hydrogen-bond strength as given by the O···H and O···O distances determined by single-crystal diffraction studies has been established.[94-96] By identifying specific proton-proton proximities, rotor-synchronised 2D ^{1}H DQ MAS spectra have been shown to differentiate between distinct hydrogen-bonded structures.[48]

Applications of dipolar-mediated DQ spectroscopy are not limited to ^{1}H NMR. For example, ^{31}P-^{31}P DQ MAS

spectra have provided valuable insight into the structure of inorganic phosphates[97] and glasses[98]. In addition, Nielsen *et al* and Hong have presented dipolar analogues of the *J*-coupled ^{13}C-^{13}C DQ MAS correlation experiment described in section 5.1.[99,100] Finally, we note that Schmidt-Rohr and co-workers have elegantly demonstrated that 2D ^{13}C-^{13}C DQ spectra recorded for static samples can identify the chain conformation statistics for ^{13}C-labelled polymer samples.[101] Remembering that the frequency of a given ^{13}C resonance depends on the orientation of the CSA tensor (see section 2.1), the method relies on the fact that the adoption of a particular torsional angle along the chain results in DQ peaks for only specific pairs of ^{13}C frequencies. As illustrated in Figure 21, trans and gauche conformations lead to very different 2D DQ powder spectra, and it was thus possible to quantitatively determine the conformation statistics for a sample of amorphous poly(ethylene terephthalate) (PET).

5.3 High-Resolution ^1H Solid-State NMR

The previous section has illustrated that the resolution in a ^1H DQ MAS spectrum provided by a combination of very-fast MAS and a high magnetic field as well as the extension to a second frequency dimension is sufficient to allow the differentiation of some particular ^1H resonances. However, as noted in section 3.2, the line narrowing achieved by MAS alone at a ν_R equal to 30 kHz is still far from the limiting case, where all residual dipolar broadening has been removed. Section 3.2 also briefly introduced experiments which provide homonuclear ^1H decoupling by combining multiple (*rf)* pulse sequences with MAS. In this section, we demonstrate that a marked line narrowing as compared to MAS alone can be achieved by this CRAMPS approach.

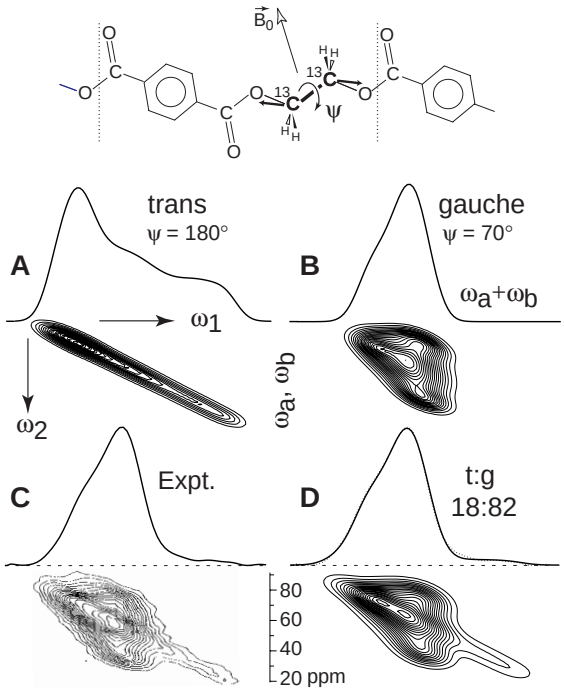

Figure 21. 2D ^{13}C-^{13}C DQ static spectra allow the determination of the chain conformation statistics for ^{13}C-labelled polymer samples. The simulated spectra show that (A) trans and (B) gauche conformations lead to very different 2D DQ powder spectra. For the experimental spectrum (C) obtained for amorphous PET, a best-fit simulation (D) revealed a 18:82 trans:gauche distribution. (Reproduced by permission of the American Association for the Advancement of Science from Ref. [101].)

In this section, we consider "windowless" homonuclear decoupling sequences. Specific examples are the Lee-Goldburg (LG) technique[102] and refinements, namely the frequency

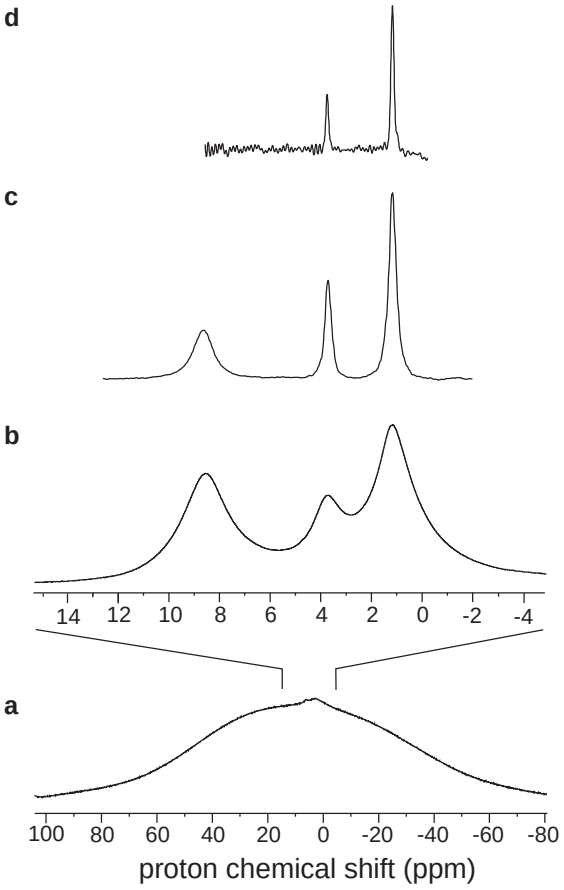

Figure 22. ^{1}H (500 MHz) NMR spectra of natural abundance powdered L-alanine, recorded with (a and b) a one-pulse experiment for (a) a static sample and (b) under MAS at a ν_R = 30 kHz, (c) the 2D FSLG (ν_R = 12.5 kHz) experiment, and (d) the CT-CRAMPS (ν_R = 12.5 kHz) experiment using FSLG decoupling. (Reproduced by permission of the American Chemical Society from Ref. [107].)

switched and phase-modulated LG (FSLG[103,104] and PMLG[105]) sequences, as well as the computer-optimised sequence, DUMBO-1[106]. For a discussion of these different decoupling sequences, the interested reader is referred to, e.g., Ref. [7]. Such sequences are so-called because no windows during which acquisition of the FID would be possible are built into the sequence. NMR experiments incorporating evolution under the application of a windowless homonuclear decoupling are thus inherently multi-dimensional. For example, Vinogradov *et al* have presented a 2D experiment in which a high-resolution ^{1}H dimension, incorporating PMLG homonuclear decoupling, is correlated with ^{1}H acquisition, with only moderate MAS (10-15 kHz) providing line narrowing in the direct dimension.[105]

Using Lee-Goldburg based decoupling methods, a FWHMH of 150-170 Hz has been reported for the aliphatic ^{1}H resonances in L-alanine[107]; this is demonstrated in part (c) of Figure 22, where, for comparison, the (a) static and (b) MAS (ν_R = 30 kHz) spectra are also shown. Lesage *et al* have further shown that the frontiers of high-resolution ^{1}H solid-state NMR can be pushed back yet further; using the constant-time (CT) CRAMPS experiment,[107] a FWHMH as low as 60 Hz can be obtained for the aliphatic resonances in L-alanine (see Figure 22 (d)).

5.4 Anisotropic-Isotropic Correlation: The Measurement of CSAs

In section 3.1, it was stated that it is possible to extract the anisotropy and asymmetry of the CSA by fitting the observed MAS sideband intensities. It is, however, necessary to be able to resolve, at a low ν_R, the sidebands of the different resonances. The problem of the 1D spectrum becoming increasingly more crowded as the number of distinct resonances increases can be overcome by

extending the NMR experiment to a second dimension.

In a first class of experiment, a 2D spectrum is obtained in which a separate anisotropic powder lineshape (corresponding to either the static case or a slow spinning frequency) is associated with each resolved resonance in an isotropic dimension. Two elegant approaches have been presented by which this can be achieved, namely magic-angle hopping (MAH)[108] and magic-angle turning (MAT)[109]. In the MAH experiment, t_1 consists of the sample making three hops of 120° about an axis inclined at the magic angle to B_0, with a period of evolution of the same incremented duration (during which the sample is static) before each hop. In this way, the evolution periods correspond to each crystallite adopting three orthogonal positions relative to B_0; for this case, it can be shown that the average chemical shift evolution equates to the isotropic chemical shift. The same effect is achieved in the MAT experiment under conditions of very slow (typically < 100 Hz) continuous sample rotation by rotations in spin space, i.e., by the application of *rf* pulses. Moreover, related experiments such as switched angle sample spinning (SASS)[110,111] and variable angle correlation spectroscopy (VACSY)[112], which involve a change in the orientation of the rotor axis with respect to B_0, have also been presented.

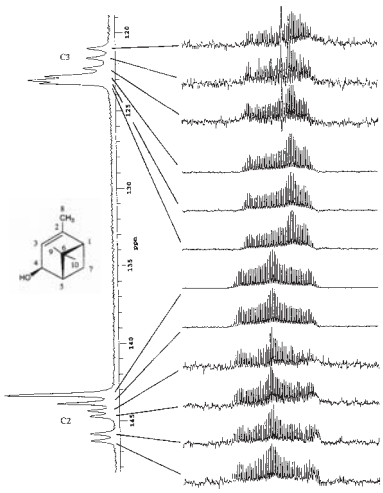

Figure 23. The anisotropic CSA patterns for each resolved resonance in a selected region of the isotropic ^{13}C spectrum as obtained from a FIREMAT experiment recorded for a sample of the terpene verbenol. (Reproduced by permission of the American Chemical Society from Ref. [115].)

For the original MAH and MAT techniques, a significant drawback was the long measuring time (1-2 days) that was required even when up to 5 g of sample was used. However, modified versions of the MAT approach employing 180° rather than 90° pulses and using a faster ν_R have been presented, which offer a better experimental sensitivity.[113,114] For example, Figure 23 shows the anisotropic CSA patterns for each resolved resonance in a selected region of the isotropic ^{13}C spectrum of the terpene verbenol.[115] Six resonance lines are resolved for both the C2 and C3 carbons, with the CSA tensor spinning-sideband patterns being remarkably similar. Supported by quantum-chemical calculations of the ^{13}C

CSA tensors, the solid-state NMR analysis demonstrated that verbenol exhibits polymorphism, with there, however, only being minor conformational variations in the distinct solid-state environments. It is to be noted that single crystals suitable for an X-ray diffraction analysis could only be obtained for the major crystalline form.

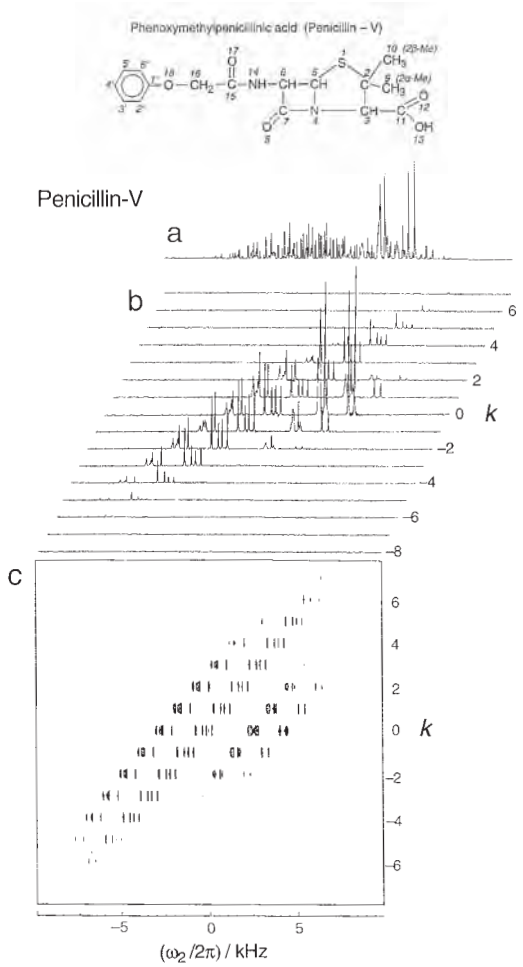

Figure 24. A 2D ^{13}C PASS spectrum recorded for the antibiotic, penicillin-V. The 1D CP MAS spectrum is shown in (a). (Reproduced by permission of Academic Press from Ref. 117.)

An alternative means by which the isotropic and anisotropic chemical shift interactions can be separated is the 2D PASS (phase-adjusted spinning sidebands) experiment due to Levitt and co-workers.[116] By changing the timings of the application of five π pulses in the t_1 dimension, it is possible to separate the spinning sidebands by order. As a specific example, Figure 24 shows the 2D ^{13}C PASS spectrum for the antibiotic, penicillin-V.[117] An analysis of this spectrum allowed the determination of the CSA principal values for all the ^{13}C resonances. A distinct advantage of this approach is that only very few (typically 16) increments must be made in the indirect dimension.

5.5 The Investigation of Slow Dynamics: 2D Exchange

The basic principle of 2D exchange NMR involves the measurement of the frequency of the same molecular segment at two different times. A slow dynamic process is detected on account of the change, during a mixing time between the two evolution periods, in the NMR frequency caused by a reorientation of the molecular segment. In this section, we describe ^{2}H static and ^{13}C MAS 2D exchange experiments.[4]

In static ^{2}H 2D exchange NMR, advantage is taken of the simplification resulting from both the presence of a single ^{2}H resonance and the fact that the quadrupolar interaction dominates (see section 2.4). Without any slow dynamics in the mixing time, the frequency of each molecular segment remains unchanged, and the intensity in the 2D frequency-domain spectrum is restricted to a ridge

along the $\nu_1 = \nu_2$ diagonal. If a reorientation occurs, off-diagonal intensity is observed as a consequence of the frequency change. In particular, a well-defined motion yields an elliptical off-diagonal pattern which is characteristic of the reorientation angle. The beauty of the static ^{2}H exchange experiment is illustrated in Figure 25, which shows a spectrum recorded for a sample of methyl-deuterated isotactic polypropylene (iPP).[118] The observed elliptical ridges are characteristic of the helical chain reorientation illustrated in the inset.

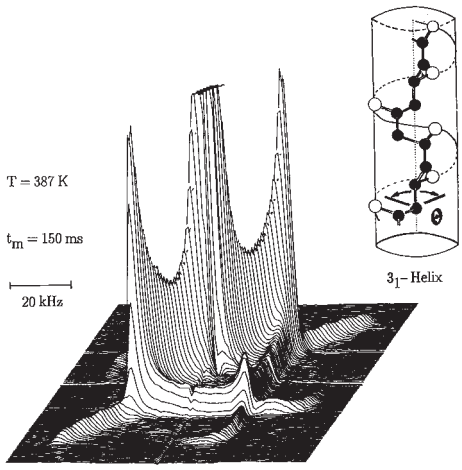

Figure 25. A static ^{2}H exchange experiment recorded for a sample of methyl-deuterated isotactic polypropylene (iPP) at T = 387 K. The observed elliptical ridges are characteristic of the helical chain reorientation illustrated in the inset. (Reproduced by permission of the American Chemical Society from Ref. [118].)

A 2D exchange experiment can also be recorded under MAS, although care must be taken to ensure that pure absorption-mode spinning sidebands are obtained. As compared to a static experiment, both the resolution and sensitivity is improved, which is of much importance for ^{13}C NMR. These gains are, however, at the expense of the ease with which information about the reorientation process can be accessed. As in the static case, a reorientation is associated with the observation of off-diagonal intensity. As a specific example, Figure 26 presents a ^{13}C 2D MAS exchange spectrum recorded for polyoxymethylene (POM).[119] In addition to probing the motion of a particular molecular moiety, 2D exchange experiments are well suited to the investigation of slow chemical exchange processes; for example, Titman *et al* have studied the hydrogen shift and/or π flip which occurs in solid tropolone.[120]

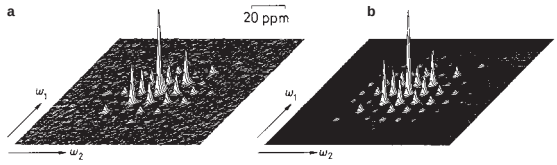

Figure 26. (a) Experimental and (b) theoretical ^{13}C 2D MAS pure absorption-mode exchange spectra recorded for polyoxymethylene (POM). The experimental spectrum corresponded to T = 360 K and a mixing time of 1.5s. (Reproduced by permission of Academic Press from Ref. [119].)

5.6 ^{1}H-^{1}H DQ MAS Spinning-Sideband Patterns

In section 5.2, a rotor-synchronised ^{1}H-^{1}H DQ MAS spectrum was presented (Figure 20). The 2D DQ MAS can be performed in an alternative fashion; if the t_1 increment is reduced, which corresponds to an increase in the DQ spectral width, a DQ MAS spinning-sideband pattern is observed.[121,122] Such DQ MAS sideband patterns exhibit characteristic unusual

features. In particular, the observed patterns are very sensitive to the product of the dipolar coupling constant, *D*, and the recoupling time, τ_{rcpl}, with an increase in this product leading to the appearance of higher-order spinning sidebands.

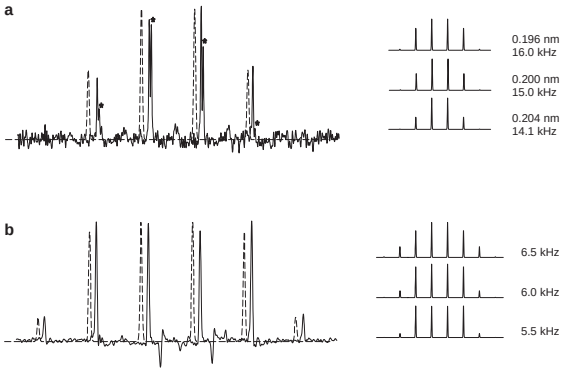

Figure 27. Extracted columns from ^{1}H (500.1 MHz) DQ MAS spectra of HBC-C_{12}, showing the DQ spinning sideband patterns for (a) the aromatic protons at 8.3 ppm in the solid phase (T = 333 K), and (b) the aromatic protons at 6.2 ppm in the LC phase (T = 386 K). In each case, best-fit spectra, generated according to the analytical expression for a spin pair, are shown (shifted to the left to allow a better comparison) as dotted lines. A spinning frequency, ν_R, equal to 35 and 10 kHz was used for the solid and LC phases, respectively, with the two rotor-period compensated BABA recoupling sequence being used for the excitation and reconversion of DQCs in both cases. In (a), additional peaks corresponding to DQCs between aromatic and residual undeuterated α-carbon protons are marked by *. The insets to the right of the experimental spectra show the sensitivity of the spinning-sideband patterns to the product $D\ \tau_{rcpl}$. (Reproduced by permission of the American Chemical Society from Ref. 49.)

Importantly, since τ_{rcpl} is known, the absolute value of *D* can be extracted by an analysis of DQ MAS spinning-sideband patterns. As a specific example, Figure 27 presents experimental ^{1}H-^{1}H DQ MAS spinning sideband patterns for the aromatic protons in (a) the crystalline and (b) the LC phases of the same alkyl-substituted polycyclic aromatic system, HBC-C_{12}, discussed in section 5.2.[49] The dotted lines represent best-fit spectra simulated using the analytical time-domain expression for an isolated spin pair. As is evident from the insets on the right of Figure 27, the DQ MAS spinning sideband patterns are very sensitive to the product of *D* and τ_{rcpl}. The best-fit spectra for the solid and LC phases then correspond to $D/(2\pi)$s equal to 15.0 ± 0.9 and 6.0 ± 0.5 kHz, respectively.

Comparing the evaluated *D* values for the crystalline and LC phases, a reduction of *D* by a factor of 0.40 ± 0.04 is observed, corresponding to an order parameter[123] of 0.80 ± 0.08. This could be explained by postulating the presence of out-of-plane motion in addition to the axial rotation of the molecule about an axis perpendicular to the ring. The good agreement with the value of 0.84 obtained from an analysis of ^{2}H 1D NMR lineshapes is to be noted.[124] It is to emphasised, however, that the ^{1}H DQ MAS method is applicable to as synthesised samples, i.e., there is no reliance upon isotopic labelling.

As well as the investigation of dynamics, an analysis of ^{1}H DQ MAS spinning-sideband patterns can be used to determine proton-proton distances. For example, it was possible to determine that the distance between the lactam and pyrrole NH protons in the complex hydrogen-bonding arrangement in the biologically important molecule bilirubin is 0.186 ± 0.002 nm.[125] In this respect, it

is to be noted that structure determination by single-crystal X-ray diffraction methods, being based on the diffraction of X-rays by electrons, is not well suited to the localisation of lighter atoms. This is of particular relevance with regards to the localisation of hydrogen-bonded protons, in which case a neutron diffraction study is to be preferred.[126] Moreover, neutron diffraction is not the perfect solution: as well as the requirement for both larger crystals and very expensive facilities, the investigation of protons is complicated by their large incoherent cross section, such that deuteration, which may cause a change in the hydrogen-bonding arrangement, is often required. Thus, solid-state NMR methods which can provide inter-proton and proton-heteroatom distance constraints, by means of which the localisation of the important protons in the single crystal structure can be refined, are of much value.

Finally, we note that 1D DQ-filtered MAS experiments (corresponding to setting $t_1 = 0$) can also provide insight into dynamic processes. The principle, in this case, is that signal is only observed for pairs of protons which remain dipolar coupled for the timescale of the experiment, which in this case is the time required to excite and reconvert the DQC. For example, in Ref. [127], the kinetics of hydrogen bond breaking and formation is quantitatively analysed for a carboxylic acid dimer on the basis of the fall off in the DQ intensity with increasing temperature.

6 HETERONUCLEAR TWO-DIMENSIONAL EXPERIMENTS

6.1 Heteronuclear Correlation

In a 2D heteronuclear correlation (HETCOR) experiment, the t_1 and t_2 periods correspond to the evolution of SQC of two different nuclei, e.g., ^{1}H and ^{13}C. A number of different HETCOR experiments have been proposed which differ with respect to, e.g., the means by which coherence transfer is achieved, the type of coherence which evolves during t_1, as well as the application of homonuclear decoupling sequences.

One of the simplest HETCOR experiments is the ^{1}H-^{13}C WISE (wideline separation) experiment.[128] After the t_1 period, during which ^{1}H transverse magnetisation created by a 90° pulse evolves, coherence transfer to ^{13}C SQC, which is detected in t_2, is achieved by a simple CP step. The experiment is performed under MAS. At a low to moderate ν_R, a wide dipolar-broadened ^{1}H lineshape in F_1 (see section 3.2) is correlated with a narrow resonance line in a well-resolved isotropic ^{13}C dimension (F_2). Remembering that motion leads to a narrowing of the ^{1}H resonance due to the reduction in the dipolar broadening, the WISE experiment has found a number of applications in polymer chemistry on account of its ability to distinguish between rigid and mobile chemical moieties.[4] For example, in Figure 28, narrow and broad lines in the ^{1}H

dimension are observed for the resonances due to the mobile poly(butyl methacrylate) (PbuA) and the rigid PMMA, respectively, in a core-shell system.[129] Furthermore, as illustrated by the investigation of onion cell-wall material in Ref. [47], the information provided by WISE spectra complements that yielded by an analysis of ^{13}C T_1 and the ^{1}H $T_{1\rho}$ relaxation times.

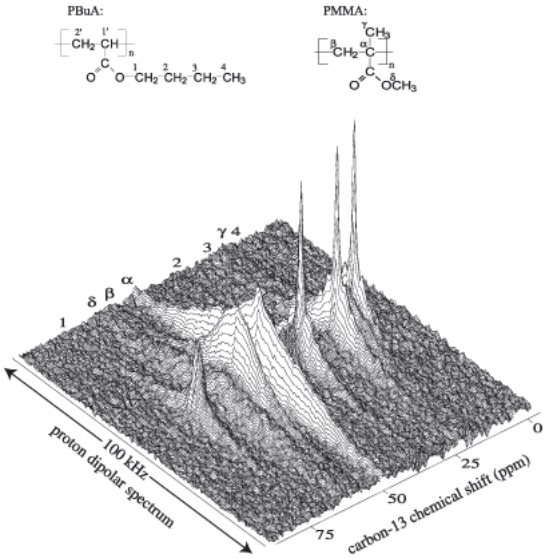

Figure 28. A ^{1}H-^{13}C WISE experiment recorded for a core-shell system comprising mobile poly(butyl methacrylate) (PbuA) and rigid PMMA. (Reproduced by permission of the American Chemical Society from Ref. [129].)

^{1}H-^{13}C HETCOR spectra incorporating a high-resolution ^{1}H dimension can be achieved. As early as 1982, Caravatti *et al* presented an experiment which employed a multiple-pulse sequence at a low ν_R (as in the conventional CRAMPS approach) to achieve homonuclear decoupling in t_1.[130,131] Recently, various alternative high-resolution HETCOR experiments applicable at a fast or a very-fast ν_R have been proposed. Two methods which utilise the through-space dipolar coupling to achieve coherence transfer are those due to van Rossum *et al*[132] and Saalwächter *et al*[133,134]. In the former case, coherence transfer occurs via CP, while FSLG ^{1}H homonuclear decoupling (see section 5.3) is applied during the evolution of transverse ^{1}H magnetisation in t_1. This is to be compared with the latter recoupled polarisation transfer (REPT) methods, which employ REDOR recoupling under very-fast MAS (see section 4.1) to create a heteronuclear SQC (HSQC) or a heteronuclear MQC (HMQC), the evolution of which is followed during t_1. The analogy to the well-known solution-state heteronuclear single-quantum correlation (HSQC)[135] and heteronuclear multiple-quantum correlation (HMQC)[136] experiments (dilute-spin, e.g. ^{13}C, detected) is to be noted.

Alternatively, the MAS-*J*-HMQC[137,138] and MAS-*J*-HSQC experiments[139] utilise the isotropic through-bond *J* coupling. The primary aim of recording a ^{1}H-^{13}C correlation spectrum is usually the establishing of one-bond correlations, such that the ^{1}H chemical shifts can be identified. For correlation methods based on the dipolar coupling, it is necessary to ensure that the observed peaks are then not due to close through-space proximities. This problem is obviously avoided by utilising through-bond *J* couplings. As an example, Figure 29 presents ^{1}H-^{13}C and ^{1}H-^{15}N MAS-*J*-HMQC spectra recorded for 20 mg of a tripeptide sample at natural abundance.[138]

The recording of ^{1}H-^{13}C MAS-*J*-HMQC spectra which reveal one- and multiple-bond connectivities allowed the complete assignment of the ^{1}H, ^{13}C, and ^{15}N resonances for the tripeptide.

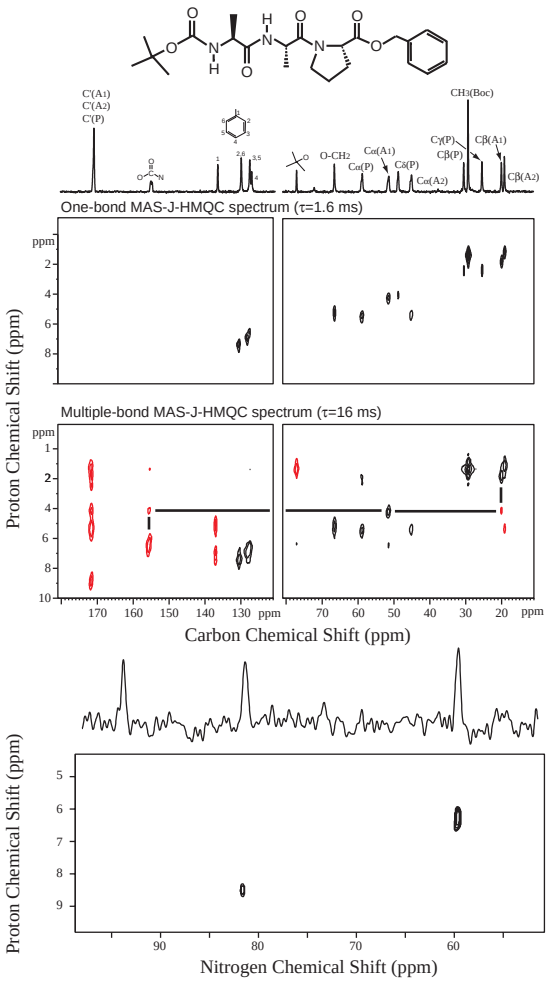

Figure 29. ^{1}H-^{13}C and ^{1}H-^{15}N MAS-*J*-HMQC spectra recorded for a tripeptide sample at natural abundance. Two different ^{1}H-^{13}C experiments were performed, with the use of a short (τ = 1.6 ms) and a long (τ = 16 ms) evolution period selecting in the former case one-bond correlations, while the latter case allowed the identification of multiple-bond correlations. ^{13}C and ^{15}N CP MAS spectra are presented above the relevant 2D spectra. (Reproduced by permission of the American Chemical Society from Ref. [138].)

It should be noted that the existence of methods based on both dipolar and *J* couplings opens up the possibility for distinguishing through-bond connectivities and through-space proximities on a medium- to long-range, such that insight into intermolecular packing arrangements is provided. In this way, the two approaches are complimentary in a similar way to the case of the COSY and NOESY[1,2] solution-state NMR experiments.

6.2 The Quantitative Determination of Heteronuclear Dipolar Couplings

As described in section 4.1, the REDOR experiment, by allowing the quantitative determination of dipolar couplings, accurately yields the distance between two heteronuclei. Indeed, REDOR is currently the workhorse experiment for structure determination. The method does, however, rely on selective isotopic labelling. As well as measuring internuclear distances, section 5.6 showed how probing the change in the dipolar coupling provides insight into a dynamic process. In this section, 2D experiments which have the aim of measuring multiple heteronuclear dipolar couplings (as opposed to only one in the REDOR experiment) are described.

In a separated local field (SLF) experiment,[140-143] the basic principle is that a spinning-sideband pattern, from which the heteronuclear dipolar coupling can be extracted, is obtained in the indirect dimension for each resolved resonance in the direct dimension, i.e., the dipolar interaction is separated from the chemical shift interaction (the experiment is

sometimes referred to as the DIPSHIFT experiment). In the original SLF papers, a homonuclear decoupling method is applied in t_1, but recently McElheny *et al* have shown that fast MAS alone at a ν_R of at least 12 kHz (much faster MAS should be avoided since the higher-order spinning sidebands become too weak to allow a reliable fitting) provides sufficient proton dipolar decoupling such that relatively reliable ^{1}H-^{13}C dipolar couplings can be extracted.[144]

Alternatively, in a modification of the original SLF method, Hohwy *et al* have presented a sophisticated experiment in which a pulse sequence is applied during t_1 which actively recouples the weak heteronuclear dipolar coupling while decoupling the homonuclear ^{1}H-^{1}H dipolar coupling.[145] Instead of giving a spinning-sideband pattern, a powder line shape is obtained in the indirect dimension. It is shown that this experimental approach allows the accurate determination of both N-H distances as well as the H-N-H bond angle in a NH_2 group. Another state-of-the-art method which has recently been proposed involves performing CP from ^{1}H to ^{13}C with the *rf* pulse on the ^{1}H channel fulfilling the Lee-Goldburg condition mentioned in section 5.3.[146] The suppression of the homonuclear ^{1}H dipolar couplings means that a LG-CP signal builds up in an oscillatory manner, reflecting coherent heteronuclear transfer. The Fourier transformation of such build-up curves yields powder spectra with marked singularities from the separation of which the heteronuclear dipolar coupling can be determined. Alternatively, it is to be noted that an analysis of a standard CP build-up curve under fast MAS can, in some cases, allow the determination of the heteronuclear dipolar coupling.[147]

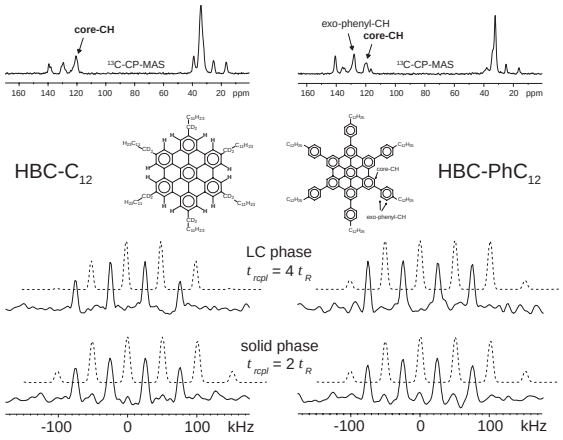

Figure 30. ^{1}H-^{13}C heteronuclear MQ MAS spinning-sideband patterns, obtained at a ν_R = 25 kHz, using the REPT-HMQC experiment. The patterns correspond to the sum projections over the ^{13}C resonance due to the aromatic core CH in the 2D spectra of HBC-C_{12}, and HBC-PhC_{12}. The spectra for the room temperature (solid) and high temperature LC phases were recorded at 35 °C and 120 °C, respectively. The dashed traces represent simulated spectra, obtained by taking into account the best-fit *D*s for the CH groups. At the top, ^{13}C CP-MAS (ν_R = 15 kHz) spectra are presented, with the signal positions of the aromatic CH resonances being identified. (Reproduced from Ref. [148].)

In direct analogy to the homonuclear DQ MAS experiment (see section 5.6), if the t_1 increment in the REPT pulse sequences (see section 6.1) is not set equal to τ_R, a spinning-sideband pattern rotor-encoded by the heteronuclear dipolar coupling is obtained.[133,134,148] An advantage of the heteronuclear ^{1}H-^{13}C approach is that it benefits from the better resolution in a ^{13}C SQ dimension. An example of this is provided by the hexa(*para*-*n*-dodecylphenyl)-substituted

HBC (henceforth referred to as HBC-PhC_{12}).[148] In this case, ^{1}H solid-state NMR is unable to distinguish the core and exo-phenyl protons. By comparison, as shown in the ^{13}C CP MAS spectrum at the top right of Figure 30, the corresponding ^{13}C resonances are well resolved. It is, thus, possible to use the heteronuclear approach to probe separately the dynamics of the core and the outer phenyl rings. For example, the right-hand-side of Figure 30 presents ^{1}H-^{13}C spinning-sideband patterns obtained at the core aromatic CH ^{13}C resonance for the solid and LC phases of HBC-PhC_{12}, using the REPT-HMQC experiment.

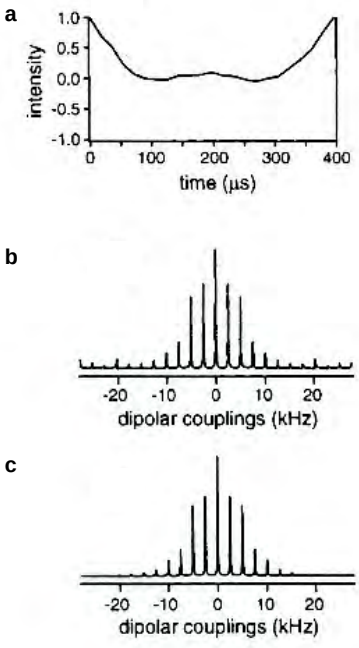

Figure 31. The measurement of the H^{N}-N-C^{α}-H^{α} torsional angle in ^{15}N-labelled NAV. The (a) t_1 FID and (b) frequency-domain spinning-sideband pattern depend on the evolution under the N-H^{N} and C^{α}-H^{α} dipolar coupling, and in particular the relative orientation of the two bonds. The (c) best-fit simulation corresponds to a torsional angle of −135°. (Reproduced by permission of the American Chemical Society from Ref. 150.)

A comparison of the spinning-sideband patterns obtained for the LC phases of HBC-C_{12} and HBC-PhC_{12} reveals that the third-order spinning sidebands are significantly higher in the latter case; they are of the same height as the first-order spinning sidebands for HBC-PhC_{12}. Since the same experimental conditions were used in both cases, this result immediately indicates a larger dipolar coupling and, hence, a larger order parameter for HBC-PhC_{12}. Indeed, the order parameter is determined to be 0.93 ± 0.09, indicating less out-of-plane mesogen mobility. It is interesting that this NMR result is correlated with an improved intra- and intercolumnar packing as evidenced by powder X-ray diffraction patterns.[148]

6.3 Torsional Angles

In an extension to experiments which measure internuclear distances, Levitt and co-workers and Griffin and co-workers have presented ingenious methods which allow the measurement of torsional angles.[149,150] The methods involve the creation of MQC between a pair of nuclei (selective isotopic labelling is required), which may be homonuclear, e.g. ^{13}C-^{13}C, or heteronuclear, e.g. ^{13}C-^{15}N. A spinning-sideband pattern is observed due to the evolution of the 2 spins which make up the MQC under the dipolar couplings to the directly attached nuclei. As a specific example, consider the H^{N}-N-C^{α}-H^{α} moiety in ^{15}N-labelled NAV.[150] By incrementing a period of ^{1}H homonuclear decoupling, a t_1 FID (Figure 31 (a)) is

obtained which depends on the evolution under the N-H^N and C^α-H^α dipolar coupling, and in particular the relative orientation of the two bonds. From the best-fit simulation (Figure 31 (c)) of the experimental frequency-domain spinning-sideband pattern (Figure 31 (b)), the torsional angle was determined to be −135°.

6.4 Oriented Samples

The difficulties associated with the preparation of samples suitable for diffraction studies has led to much interest in the application of solid-state NMR to the investigation of the three-dimensional structure adopted by membrane proteins in their functional environment of phospholipid bilayers.[14] As an oriented sample, the NMR spectrum of a membrane protein is much simplified as compared to the case of a powder sample; for perfect ordering, all structurally equivalent nuclei have the same orientation with respect to B_0, and hence the same anisotropic resonance frequency (see section 2.1). This phenomenon is taken advantage of in the PISEMA (polarisation inversion with spin exchange at the magic angle) experiment.[151] This technique is closely related to the experiments described in section 6.2, although it is to be noted that it is applied to static samples.

Figure 32 (a) presents a 2D PISEMA spectrum of a uniformly ^{15}N-labelled polypeptide in an oriented lipid bilayer.[152] For each ^{15}N resonance, the ^{15}N chemical shift (horizontal axis) is correlated with the corresponding ^{15}N-^{1}H dipolar coupling, with both the chemical shift and the dipolar coupling depending on the orientation of the particular nitrogen containing moiety. Making the assumption that the local chemical environment leads to only slight variations in the principal values and orientations of the CSA and dipolar tensors, the observed PISEMA pattern allows the tilt angle of the polypeptide helix with respect to the bilayer normal to be determined. For example, the best-fit simulated spectrum in Figure 32 (b) corresponds to a helix tilt angle of 12°.

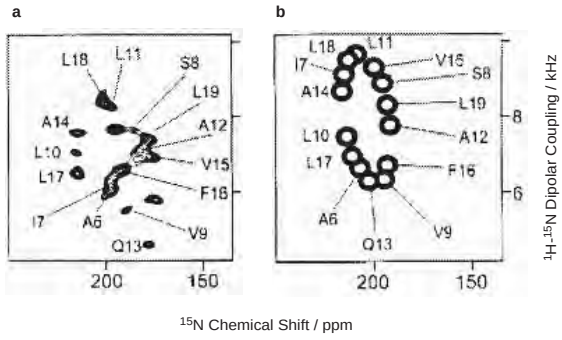

Figure 32. (a) A 2D PISEMA spectrum of a uniformly ^{15}N-labelled polypeptide in an oriented lipid bilayer. (b) The best-fit simulated spectrum corresponds to a helix tilt angle of 12°. (Reproduced by permission of Academic Press from Ref. [152].)

PISEMA experiments yield the local dipolar field experienced by the ^{13}C or ^{15}N nucleus. Perhaps counter intuitively, it has been shown that better resolution is obtained by using experiments which detect the local dipolar field on protons.[130,153,154,155] As specific examples, the ^{1}H detected local field experiment has recently successfully been

applied to the characterisation of liquid crystals[156,157] and membranes[158]. As illustrated by Figure 33, this approach has even been shown to yield sufficient resolution in 3D versions to allow the direct measurement of internuclear dipolar couplings between nuclei separated by up to five bonds in liquid crystals, thereby providing very strong conformational constraints.[159]

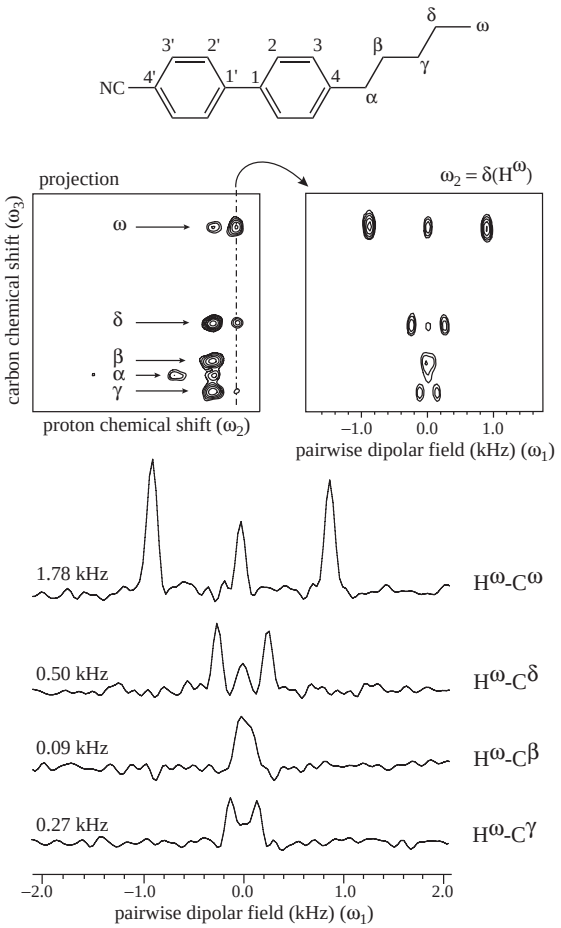

Figure 33. The aliphatic region of the 3D pairwise local field spectrum of the nematic LC, 5CB. A projection onto the $\omega_2 - \omega_3$ plane yields a ^{1}H-^{13}C correlation spectrum (upper left), and a plane taken perpendicular to this at a particular ^{1}H chemical shift yields a $\omega_3 - \omega_1$ slice (upper right) that contains a series of pairwise local fields for each carbon atom. The pairwise local fields obtained for Hω are shown, which demonstrate that couplings to carbons all the way down the chain to Cβ can be measured. (Reproduced by permission of the American Chemical Society from Ref. [159].)

7 HALF-INTEGER QUADRUPOLAR NUCLEI

An inspection of Table 2 reveals that many nuclei of relevance in inorganic systems, e.g. ^{23}Na (spin I = 3/2), ^{27}Al (spin I = 5/2), and ^{17}O (spin I = 5/2), are quadrupolar with a half-integer nuclear spin. For such nuclei, an important result is that the $|m_I = +s\rangle \leftrightarrow |m_I = -s\rangle$ transitions are not broadened by the quadrupolar coupling to first order (for a spin I = 3/2 nucleus, the energy levels are labelled –3/2, –1/2, +1/2, and + 3/2). As a consequence, for the usual case that the quadrupolar coupling is large (typically on the order of MHz), only the central transition, $|m_I = +1/2\rangle \leftrightarrow |m_I = -1/2\rangle$, is observed in the normal spectrum, since the broadened satellite transitions ($|m_I = +3/2\rangle \leftrightarrow |m_I = +1/2\rangle$ and $|m_I = -1/2\rangle \leftrightarrow |m_I = -3/2\rangle$ for a spin I = 3/2 nucleus) are lost in the baseline. It should be noted that various groups have presented ingenious methods which use the satellite transitions to enhance the sensitivity of the central transition spectrum.[160-162]

The central transition of a half-integer quadrupolar nucleus is, however, broadened to second order. In contrast to the CSA, and dipolar and first-order quadrupolar couplings, the orientation dependence of the broadening associated with second-order quadrupolar coupling is no longer purely a second-rank tensor. In particular, there is a fourth-rank tensor contribution, which is not fully removed

by MAS (regardless of what ν_R is used). The residual second-order quadrupolar broadening of the central transition often prevents the resolution of resonances due to chemically or crystallographically distinct sites.[163] For example, Figure 34 (b) shows the ^{87}Rb (spin I = 3/2) MAS spectrum of $RbNO_3$; the presence of residual second–order quadrupolar broadening precludes the resolution of the three crystallographically distinct sites.

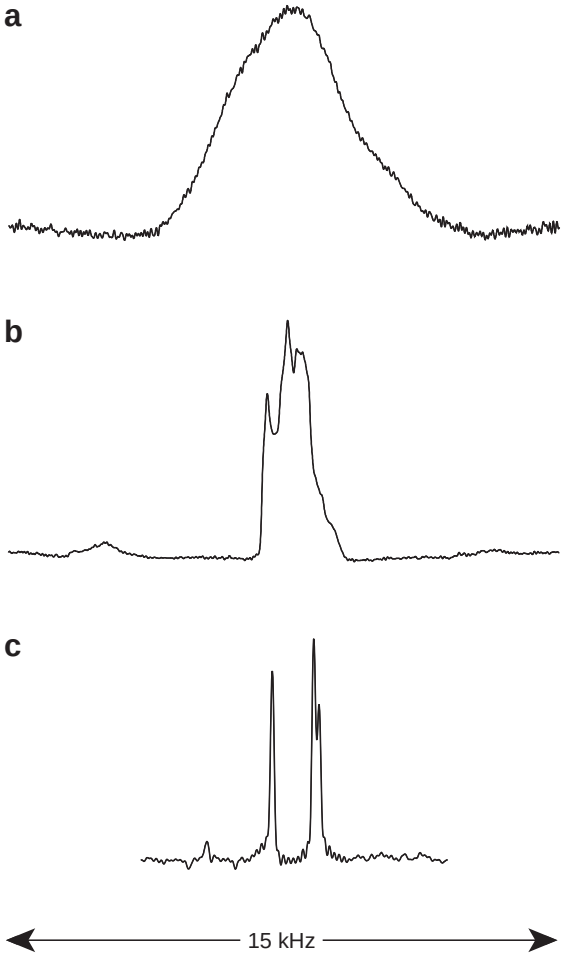

Figure 34. ^{87}Rb (130.9 MHz) (spin I = 3/2) (a) static, (b) MAS, and (c) isotropic MQMAS spectra of $RbNO_3$.

Since the fourth-rank anisotropic broadening can be removed by sample rotation at an angle of 30.6° or 70.1° with respect to B_0, high-resolution spectra corresponding to the removal of the residual second-rank quadrupolar broadening can be achieved by the methods of double rotation (DOR)[164] and dynamic-angle spinning (DAS)[165], which, respectively, involve the simultaneous and sequential rotation of the sample about two axes.[166] As a specific example, Figure 35 (a) presents a ^{17}O 2D DAS spectrum of the bridging oxygen (Si-O-Si) resonances in a $K_2Si_4O_9$ glass.[167,168] Residual second-order quadrupolar broadening is removed from the isotropic dimension such that the broadness of the isotropic lineshape reflects a continuous variation in the ^{17}O isotropic frequency. The selected anisotropic cross sections demonstrate that the quadrupolar coupling parameters vary as the isotropic frequency changes. In combination with quantum chemical calculations, the information about the ^{17}O quadrupolar interactions allows the determination of the Si-O-Si bond angle

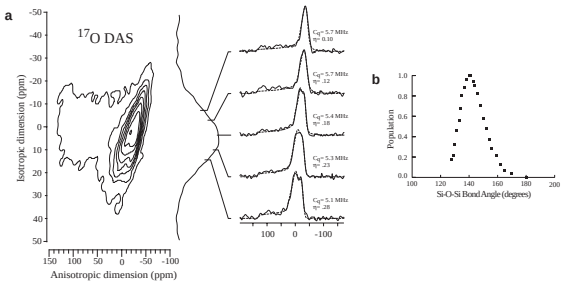

Figure 35. (a) A ^{17}O 2D DAS spectrum of the bridging oxygen (Si-O-Si) resonances in a $K_2Si_4O_9$ glass. Selected anisotropic cross sections corresponding to different ^{17}O isotropic frequencies are shown. (b) The Si-O-Si bond angle distribution in the glass, as determined by the use of quantum chemical calculations to interpret the experimental information about the ^{17}O quadrupolar interactions. (Reproduced from Ref. 168.)

distribution in the glass (Figure 35 (b)). Although a number of impressive applications of both the DAS and DOR methods have been presented, the technical complexity of both experiments has meant that their use is not widespread.

In 1995, Frydman and Harwood presented a 2D MQMAS experiment, which, by means of the formation of an echo corresponding to the refocusing of the fourth-rank second-order quadrupolar broadening, yields 2D spectra in which anisotropically broadened ridges are resolved on the basis of their different isotropic shifts.[169] The resolution of the three distinct Rb sites in $RbNO_3$ in an isotropic MQMAS spectrum is demonstrated in Figure 34 (c). It is to be noted that the experiment is only applicable for odd MQ orders (e.g. 3Q or 5Q), for which there is no first-order quadrupolar broadening. Moreover, as compared to the spin $I = 1/2$ MQ methods described earlier in this article, MQC can be excited for a single isolated nucleus.

The MQ MAS technique has the big advantage of requiring only conventional MAS hardware. In the last five years, much attention has been devoted to the optimisation of the technique, with respect to e.g., obtaining pure absorption-mode lineshapes, improving the sensitivity, and extending the applicability to nuclei with ever greater quadrupolar couplings; various groups have carried out studies to compare the different variants which have been proposed.[170-172] The development has been so rapid that MQMAS NMR of nuclei such as ^{23}Na, ^{27}Al and ^{17}O can now be considered to be routine, with many applications having been presented, which encompass, e.g., glasses, minerals, and microporous materials.[173-178]

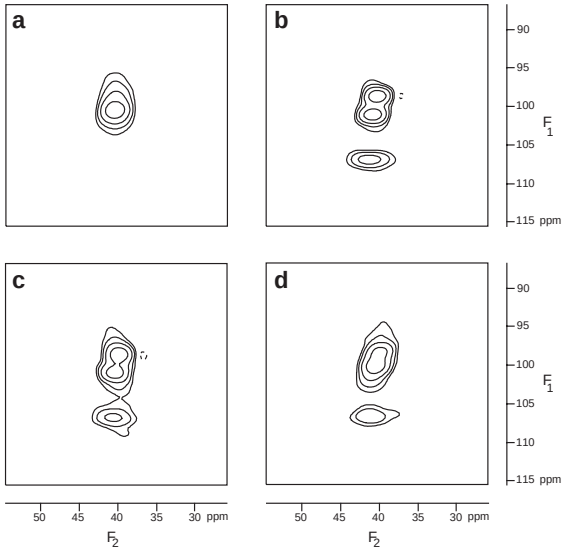

Figure 36. ^{27}Al (104.3 MHz) 5Q MAS spectra corresponding to the tetrahedral aluminium sites in the microporous aluminium methylphosphonates (a) AlMePO-α and (b) AlMePO-β, as well as (c) a physical mixture of the two forms, and (d) a sample in which the thermal transformation between the two forms was interrupted. (Reproduced by permission of the American Chemical Society from Ref. [176].)

As a specific example, Figure 36 shows ^{27}Al 5Q MAS spectra corresponding to the tetrahedral aluminium sites in the microporous aluminium methylphosphonates (a) AlMePO-α and (b) AlMePO-β.[176] In Figure 36 (b), three distinct sites can be distinguished in the isotropic (F_1) dimension. In a MAS experiment (this corresponds to the projection onto the F_2 dimension), only a single peak is observed in the tetrahedral region. AlMePO-β can be converted by a

thermal transformation into AlMePO-α. As discussed in Ref. [176], insight into this process is provided by the subtle but significant differences between the 5Q MAS spectra for a physical mixture of the two forms (Figure 36 (c)) and for a sample in which the thermal transformation was interrupted (Figure 36 (d)).

8 SUMMARY

This article has given an overview of the wide range of solid-state NMR experiments available today. The central role of anisotropic interactions, e.g. the CSA and the dipolar and quadrupolar couplings, has become evident. Through the orientation dependence imparted to the resonance frequency, access is made available to valuable structural and dynamic information. However, for a powder sample, the associated line broadening hinders the resolution of distinct sites. Achieving high-resolution NMR while retaining access to the information inherent to the anisotropic interactions particular to the solid state is a key aim of many of the described experimental methods.

A number of NMR methods applicable to small amounts (10-20 mg) of a powdered sample at natural abundance have been presented. In particular, recent advances in both NMR hardware and the development of new pulse sequences means that ^{1}H solid-state NMR is becoming routinely feasible. In this way, insight into the structure and dynamics of, in particular, hydrogen-bonded systems as well as aromatic π-π interactions can be provided. A further important new class of experiments are those who exploit the *J* coupling to establish through-bond connectivities. As a general strategy, as much information as possible should be first gleaned for the sample at natural abundance (for large biological systems, global isotopic labelling is unavoidable). If pertinent questions remain unanswered, a strategy involving the synthesis of a sample incorporating selective isotopic labelling can be considered.

Solid-state NMR spectroscopy should certainly not be used in isolation. For example, the assignment of solid-state spectra is aided by the existence of solution-state NMR spectra, while if dynamic processes are to be investigated, it is very useful if differential scanning calorometry (DSC) curves can be first obtained, so that the temperatures at which phase transitions occur are known in advance. In addition, the advances in computing power as well as the development of methodology means that the use of quantum chemical calculations of NMR parameters in the interpretation of experimental results will become ever more popular.

Solid-state NMR should not be considered as a replacement for the established diffraction methods. Instead, the two methods should be thought of as being complementary, since they have much to offer each other. For example, the

existence of a single-crystal X-ray structure for a related system aids the interpretation of NMR spectra obtained for a system, where it is not possible to obtain a single crystal suitable for an X-ray analysis. In addition, solid-state NMR is of use when an X-ray single-crystal structure is available. For example, since structure determination by single-crystal X-ray diffraction methods, being based on the diffraction of X-rays by electrons, is not well suited to the localisation of lighter atoms, the ability of solid-state NMR to provide distance constraints, which can be used in the optimisation of a crystal structure, in particular the very relevant hydrogen-bonded part, is of much importance. Furthermore, solid-state NMR is extremely well suited to the investigation of dynamic processes. It can also detect polymorphic forms, which may be overlooked when selecting single crystals for X-ray diffraction analysis. Finally, by probing the CSA and quadrupolar interactions, solid-state NMR provides electronic information which is not accessible to X-ray studies.

Acknowledgements

SPB is supported by a Marie Curie Fellowship of the European Community programme "Improving Human Research Potential and the Socio-economic Knowledge Base" under contract number "HPMFCT-2000-00525". The information published does not represent the opinion of the Community, and the Community is not responsible for any use that might be made of data appearing therein.

APPENDIX:
Anisotropic Interactions: The Orientation Dependence of the Resonance Frequency[4]

For the CSA,

$$\omega_{cs} = \omega_0\left(\sigma_{xx}^{pas}\cos^2\phi\sin^2\theta + \sigma_{yy}^{pas}\sin^2\phi\sin^2\theta + \sigma_{zz}^{pas}\cos^2\theta\right) \quad \text{(A1)}$$

where ω_0 is the Larmor frequency, σ_{xx}^{pas}, σ_{yy}^{pas}, and σ_{zz}^{pas} are the principal values (eigenvalues) in the pas, and ϕ and θ are polar angles defining the transformation of the pas onto the laboratory frame defined by B_0.

The CSA is more commonly expressed as a sum of an isotropic and an anisotropic part. The isotropic chemical shift is given by

$$\sigma_{iso} = \tfrac{1}{3}\left(\sigma_{xx}^{pas} + \sigma_{yy}^{pas} + \sigma_{zz}^{pas}\right) \quad \text{(A2)}$$

while the anisotropic frequency is

$$\omega_{aniso} = \frac{\delta}{2}\left(3\cos^2\theta - 1 - \eta\sin^2\theta\cos 2\phi\right) \quad \text{(A3)}$$

where δ and η describe the anisotropy and the asymmetry of the interaction, respectively.

An important feature of solid-state NMR is that the orientation dependence of the CSA, dipolar, and first-order quadrupolar interactions can all be represented by what are referred to as second-rank tensors. As a consequence, eq. (A3) can be considered as a general expression which applies to all three interactions. It should be noted that the isotropic part is zero for both the dipolar coupling and the first-order quadrupolar interaction.

For the dipolar coupling between a pair of spins, the interaction is always axially symmetric and thus $\eta = 0$. It is necessary to distinguish between a heteronuclear and a homonuclear dipolar coupling. For the heteronuclear case,

$$\delta = D, \quad \text{(A4)}$$

while for the homonuclear case,

$$\delta = 3D/2, \quad \text{(A5)}$$

where D is the dipolar coupling constant:

$$D = \frac{\mu_0\hbar\gamma_I\gamma_S}{4\pi r^3} \ . \quad \text{(A6)}$$

r denotes the internuclear distance, while γ corresponds to the magnetogyric ratio.

For the first-order quadrupolar interaction,

$$\delta = \frac{3\pi C_Q}{2I(2I-1)} \ , \quad \text{(A7)}$$

where the quadrupolar coupling constant, C_Q, (in units of hertz) is given by

$$C_Q = \frac{e^2qQ}{h} \ . \quad \text{(A8)}$$

eq corresponds to the electric field gradient at the nucleus and Q to the nuclear quadrupole moment.

References

1. R. R. Ernst, G. Bodenhausen, and A. Wokaun, 'Principles of Nuclear Magnetic Resonance in One and Two Dimensions', Clarendon, Oxford, 1987.
2. T. D. W. Claridge, 'High-Resolution NMR Techniques in Organic Chemistry', Pergamon, Amsterdam, 1999.
3. M. Mehring, 'Principles of High Resolution NMR in Solids', Springer, Berlin, 1983.
4. K. Schmidt-Rohr and H. W. Spiess, 'Multidimensional Solid-State NMR and Polymers', Academic Press, New York, 1994.
5. L. Emsley, D. D. Laws, and A. Pines, Lectures on Pulsed NMR (3rd edition) In 'The Proceedings of the International School of Physics "Enrico Fermi"', Course CXXXIX, ed. B. Maraviglia, IOS Press, Amsterdam, 1999, p. 45.
6. R. K. Harris, in 'Encyclopedia of Nuclear Magnetic Resonance', eds. D. M. Grant and R. K. Harris, Wiley, Chichester, 1996, Vol. 5, p.3301.
7. S. P. Brown and H. W. Spiess, *Chem. Rev.* 2001, **101**, 4125.
8. A. E. Bennett, R. G. Griffin, and S. Vega, in 'NMR Basic Principles and Progress', Springer-Verlag, Berlin, 1994, Vol. 33, p.1.
9. S. Dusold and A. Sebald, *Ann. Rep. NMR Spectrosc.* 2000, **41**, 185.
10. M. H. Sherwood, in 'Encyclopedia of Nuclear Magnetic Resonance', eds. D. M. Grant and R. K. Harris, Wiley, Chichester, 1996, Vol. 2, p.1322.
11. R. Gerald II, T. Bernhard, U. Haeberlen, J. Rendell, and S. Opella, *J. Am. Chem. Soc.* 1993, **115**, 777.
12. R. Y. Dong, 'Nuclear Magnetic Resonance of Liquid Crystals', Springer, New York, 1994.
13. J. W. Emsley, in 'Encyclopedia of Nuclear Magnetic Resonance', eds. D. M. Grant and R. K. Harris, Wiley, Chichester, 1996, Vol. 4, p.2788.
14. J. H. Davis and M. Auger, *Prog. NMR Spectrosc.* 1999, **35**, 1.
15. J. H. Davis, K. R. Jeffrey, M. Bloom, M. I. Valic, and T. P. Higgs, *Chem. Phys. Lett.* 1976, **42**, 390.
16. V. Copié, A. E. McDermott, K. Beshah, J. C. Williams, M. Spijker-Assink, R. Gebhard, J. Lugtenburg, J. Herzfeld, and R. G. Griffin, *Biochemistry* 1994, **33**, 3280.
17. E. R. Andrew, A. Bradbury and R. G. Eades, *Nature* 1958, **182**, 1659.
18. I. Lowe, *Phys. Rev. Lett.* 1959, **2**, 285.
19. S. R. Hartmann and E. L. Hahn, *Phys. Rev.* 1962, **128**, 2042.
20. A. Pines, M. G. Gibby and J. S. Waugh, *J. Chem. Phys.* 1972, **56**, 1776.
21. J, Schaefer and E. O. Stejskal, *J. Am. Chem. Soc.* 1976, **98**, 1031.
22. M. M. Maricq and J. S. Waugh, *J. Chem. Phys.* 1979, **70**, 3300.
23. J. Herzfeld and A. E. Berger, *J. Chem. Phys.* 1980, **73**, 6021.
24. P. Hodgkinson and L. Emsley, *J. Chem. Phys.* 1997, **107**, 4808.
25. G. Metz, X. Wu, and S. O. Smith, *J. Magn. Reson. A.* 1994, **110**, 219.
26. S. Hediger, B. H. Meier, N. D. Kurur, G. Bodenhausen, and R. R. Ernst, *Chem. Phys. Lett.* 1994, **223**, 283.
27. W. T. Dixon, *J. Magn. Reson.* 1981, **44**, 220.
28. W. T. Dixon, *J. Chem. Phys.* 1982, **77**, 1800.
29. F. Bloch, *Phys. Rev.* 1958, **111**, 841.
30. A. E. Bennett, C. M. Rienstra, M. Auger, K. V. Lakshmi, R. G. Griffin, *J. Chem. Phys.* 1995, **103**, 6951.
31. M. Carravetta, M. Edén, X. Zhao, A. Brinkmann, M. H. Levitt, *Chem. Phys. Lett.* 2000, **321**, 205.
32. M. Ernst, H. Zimmermann, B. H. Meier, *Chem. Phys. Lett.* 2000, **317**, 581.
33. X. Wu, S. T. Burns, and K. W. Zilm, *J. Magn. Reson. A* 1994, **111**, 29.
34. A. Lesage, S. Steuernagel, and L. Emsley, *J. Am. Chem. Soc.* 1998, **120**, 7095.
35. J. Z. Hu, J. K. Harper, C. Taylor, R. J. Pugmire, and D. M. Grant, *J. Magn. Reson.* 2000, **142**, 326.
36. D. Sakellariou, A. Lesage, and L. Emsley, *J. Magn. Reson.* 2001, **151**, 40.
37. R. E. Botto in 'Encyclopedia of Nuclear Magnetic Resonance', eds. D. M. Grant and R. K. Harris, Wiley, Chichester, 1996, Vol. 3, p.2101.
38. R. J. Pugmire in 'Encyclopedia of Nuclear Magnetic Resonance', eds. D. M. Grant and R. K. Harris, Wiley, Chichester, 1996, Vol. 2, p.1355.

39. M. Pruski in 'Encyclopedia of Nuclear Magnetic Resonance', eds. D. M. Grant and R. K. Harris, Wiley, Chichester, 1996, Vol. 2, p.1378.
40. H. Saitô in 'Encyclopedia of Nuclear Magnetic Resonance', eds. D. M. Grant and R. K. Harris, Wiley, Chichester, 1996, Vol. 6, p.3740.
41. R. K. Harris in 'Encyclopedia of Nuclear Magnetic Resonance', eds. D. M. Grant and R. K. Harris, Wiley, Chichester, 1996, Vol. 6, p.3734.
42. W. S. Veeman in 'Encyclopedia of Nuclear Magnetic Resonance', eds. D. M. Grant and R. K. Harris, Wiley, Chichester, 1996, Vol. 6, p.3655.
43. R. H. Newman in 'Encyclopedia of Nuclear Magnetic Resonance', eds. D. M. Grant and R. K. Harris, Wiley, Chichester, 1996, Vol. 2, p.738.
44. H. C. Marsmann in 'Encyclopedia of Nuclear Magnetic Resonance', eds. D. M. Grant and R. K. Harris, Wiley, Chichester, 1996, Vol. 7, p.4386.
45. G. Engelhardt in 'Encyclopedia of Nuclear Magnetic Resonance', eds. D. M. Grant and R. K. Harris, Wiley, Chichester, 1996, Vol. 7, p.4398.
46. H. Eckert, *NMR basic principles and progress* 1994, **33**, 125.
47. S. Hediger, L. Emsley, and M. Fisher, *Carbohydr. Res.* 1999, **322**, 102.
48. I. Schnell, S. P. Brown, H. Y. Low, H. Ishida, and H. W. Spiess, *J. Am. Chem. Soc*. 1998, **120**, 11784.
49. S. P. Brown, I. Schnell, J. D. Brand, K. Müllen, and H. W. Spiess, *J. Am. Chem. Soc.* 1999, **121**, 6712.
50. S. P. Brown, I. Schnell, J. D. Brand, K. Müllen, and H. W. Spiess, *J. Mol. Struct.* 2000, **521**, 179.
51. K. Yamauchi, S. Kuroki, K. Fujii, and I. Ando, *Chem. Phys. Lett.* 2000, **324**, 435.
52. J. S. Waugh, L. M. Huber, and U. Haeberlen, *Phys. Rev. Lett* . 1968, **20**, 180.
53. U. Haeberlen and J. S. Waugh, *Phys. Rev.* 1968, **175**, 453.
54. B. C. Gerstein, R. G. Pembleton, R. C. Wilson, and L. M. Ryan, *J. Chem. Phys.* 1977, **66**, 361.
55. G. Scheler, U. Haubenreisser, and H. Rosenberger, *J. Magn. Reson.* 1981, **44**, 134.
56. G. E. Maciel, C. E. Bronnimann, and B. Hawkins, *Adv. Magn. Reson.* 1990, **14**, 125.
57. S. F. Dec, C. E. Bronnimann, R. A. Wind, and G. E. Maciel, *J. Magn. Reson.* 1989, **82**, 454.
58. J. M. Miller, *Prog. NMR Spectrosc.* 1996, **28**, 255.
59. S. Ando, R. K. Harris, J. Hirschinger, S. A. Reinsberg, and U. Scheler, *Macromolecules* 2001, **34**, 66.
60. S. L. Grage and A. S. Ulrich, *J. Magn. Reson.* 2000, **146**, 81.
61. T. Gullion, J. Schaefer, *J. Magn. Reson.* **1989**, *81*, 196.
62. T. Gullion, J. Schaefer, *Adv. Magn. Reson.* **1989**, *13*, 57.
63. T. Gullion, *Concepts Magn. Reson.* **1998**, *10*, 277.
64. S. M. Holl, G. R. Marshall, D. D. Beusen, K. Kociolek, A. S. Redlinski, M. T. Leplawy, R. A. McKay, S. Vega, and J. Schaefer, *J. Am. Chem. Soc.* 1992, **114**, 4830.
65. C. P. Grey, W. S. Veeman, and A. J. Vega, *J. Chem. Phys.* 1993, **98**, 7711.
66. T. Gullion, *Chem. Phys. Lett.* 1995, **246**, 325.
67. D. P. Raleigh, M. H. Levitt, and R. G. Griffin, *Chem. Phys. Lett.* 1988, **146**, 71.
68. M. H. Levitt, D. P. Raleigh, F. Creuzet, and R. G. Griffin, *J. Chem. Phys.* 1990, **92**, 6347.
69. X. Feng, P. J. E. Verdegem, Y. K. Lee, M. Helmle, S. C. Shekar, H. J. M. de Groot, J. Lugtenburg, and M. H. Levitt, *Solid State Nucl. Magn. Reson.* 1999, **14**, 81.
70. R. Tycko and G. Dabbagh, *J. Am. Chem. Soc.* 1991, **113**, 9444.
71. A. E. Bennett, J. H. Ok, R. G. Griffin, and S. Vega, *J. Chem. Phys.* 1992, **96**, 8624.
72. N. C. Nielsen, H. Bildsøe, H. J. Jakobsen, and M. H. Levitt, *J. Chem. Phys.* 1994, **101**, 1805.
73. Y. K. Lee, N. D. Kurur, M. Helmle, O. G. Johannessen, N. C. Nielsen, and M. H. Levitt, *Chem. Phys. Lett.* 1995, **242**, 304.
74. W. Sommer, J. Gottwald, D. E. Demco, and H. W. Spiess, *J. Magn. Reson. A* 1995, **113**, 131.
75. D. M. Gregory, G. Wolfe, T. Jarvie, J. C. Shiels, and G. P. Drobny, *Mol. Phys.* 1996, **89**, 1835.
76. R. Verel, M. Baldus, M. Ernst, and B. H. Meier, *Chem. Phys. Lett.* 1998, **287**, 421.
77. A. Brinkmann, M. Edén, and M. H. Levitt, *J. Chem. Phys.* 2000, **112**, 8539.

78. E. R. deAzevedo, W.-G. Hu, T. J. Bonagamba, and K. Schmidt-Rohr, *J. Am. Chem. Soc.* 1999, **121**, 8411.
79. E. R. deAzevedo, W.-G. Hu, T. J. Bonagamba, and K. Schmidt-Rohr, *J. Chem. Phys.* 2000, **112**, 8988.
80. J. Pauli, M. Baldus, B. van Rossum, H. de Groot, and H. Oschkinat, *Chem. Biochem.* 2001, **2**, 272.
81. A. Lesage, C. Auger, S. Caldarelli, and L. Emsley, *J. Am. Chem. Soc.* 1997, **119**, 7867.
82. A. Bax, R. Freeman, T. A. Frenkiel, *J. Am. Chem. Soc.* 1981, **103**, 2102.
83. Y.-S. Yen and A. Pines, *J. Chem. Phys.* 1983, **78**, 3579.
84. J. Baum, M. Munowitz, A. N. Garroway, and A. Pines, *J. Chem. Phys.* 1985, **83**, 2015.
85. P. J. Hore, J. A. Jones, and S. Wimperis, 'NMR: The Toolokit', Oxford University Press, Oxford, 2000.
86. A. Lesage, M. Bardet, and L. Emsley, *J. Am. Chem. Soc.* 1999, **121**, 10987.
87. R. Verel, J. D. van Beek, and B. H. Meier, *J. Magn. Reson.* 1999, **140**, 300.
88. H. Geen, J. J. Titman, J. Gottwald, and H. W. Spiess, *Chem. Phys. Lett.* 1994, **227**, 79.
89. P. Caravetti, P. Neuenschwander, and R. R. Ernst, *Macromolecules* 1985, **18**, 119.
90. C. Ochsenfeld, S. P. Brown, I. Schnell, J. Gauss, and H. W. Spiess, *J. Am. Chem. Soc.* 2001, **123**, 2597.
91. P. Lazzeretti, *Prog. NMR Spectrosc.* 2000, **36**, 1.
92. B.-J. van Rossum, G. J. Boender, F. M. Mulder, J. Raap, T. S. Balaban, A. Holzwarth, K. Schaffner, S. Prytulla, H. Oschkinat, and H. J. M. de Groot, *Spectrochim. Acta* 1998, **A54**, 1167.
93. S. P. Brown, T. Schaller, U. P. Seelbach, F. Koziol, C. Ochsenfeld, F.-G. Klärner, and H. W. Spiess, *Angew. Chem. Int. Ed. Engl.* 2001, **40**, 717.
94. B. Berglund and R. W. Vaughan, *J. Chem. Phys.* 1980, **73**, 2037.
95. G. A. Jeffrey and Y. Yeon, *Acta Cryst.* 1986, **B42**, 410.
96. R. K. Harris, P. Jackson, L. H. Merwin, B. J. Say, and G. Hagele, *J. Chem. Soc. Faraday Trans.* 1988, **84**, 3649.
97. M. Feike, R. Graf, I. Schnell, C. Jäger, and H. W. Spiess, *J. Am. Chem. Soc.* 1996, **118**, 9631.
98. R. Witter, P. Hartmann, J. Vogel, and C. Jäger, *Solid State Nucl. Magn. Reson.* 1998, **13**, 189.
99. N. C. Nielsen, F. Creuzet, R. G. Griffin, and M. H. Levitt, *J. Chem. Phys.* 1992, **96**, 5668.
100. M. Hong, *J. Magn. Reson.* 1999, **136**, 86.
101. K. Schmidt-Rohr, W. Hu, and N. Zumbulyadis, *Science* 1998, **280**, 714.
102. M. Lee and W. I. Goldburg, *Phys. Rev. A* 1965, **140**, 1261.
103. A. Bielecki, A. C. Kolbert, and M. H. Levitt, *Chem. Phys. Lett.* 1989, **155**, 341.
104. A. Bielecki, A. C. Kolbert, H. J. M. de Groot, R. G. Griffin, and M. H. Levitt, *Adv. Magn. Reson.* 1990, **14**, 111.
105. E. Vinogradov, P. K. Madhu, and S. Vega, *Chem. Phys. Lett.* 1999, **314**, 443.
106. D. Sakellariou, A. Lesage, P. Hodgkinson, and L. Emsley, *Chem. Phys. Lett.* 2000, **319**, 253.
107. A. Lesage, L. Duma, D. Sakellariou, and L. Emsley, L. *J. Am. Chem. Soc.* 2001, **123**, 5747.
108. A. Bax, N. M. Szeverenyi, and G. E. Maciel, *J. Magn. Reson.* 1983, **52**, 147.
109. Z. Gan, *J. Am. Chem. Soc.* 1992, **114**, 8307.
110. A. Bax, N. M. Szeverenyi, and G. E. Maciel, *J. Magn. Reson.* 1983, **55**, 494.
111. T. Terao, T. Fujii, T. Onodera, and A. Saika, *Chem. Phys. Lett.* 1984, **107**, 145.
112. L. Frydman, G. C. Chingas, Y. K. Lee, P. J. Grandinetti, M. A. Eastman, G. A. Barrall, and A. Pines, *J. Chem. Phys.* 1992, **97**, 4800.
113. S. L. Gann, J. H. Baltisberger, and A. Pines, *Chem. Phys. Lett.* 1994, **210**, 405.
114. D. W. Alderman, G. McGeorge, J. Z. Hu, R. J. Pugmire, and D. M. Grant, *Mol. Phys.* 1998, **95**, 1113.
115. J. K. Harper and D. M. Grant, *J. Am. Chem. Soc.* 2000, **122**, 3708.
116. O. N. Antzutkin, S. C. Shekar, and M. H. Levitt, *J. Magn. Reson.* 1995, **A 115**, 7.
117. O. N. Antzutkin, Y. K. Lee, and M. H. Levitt, *J. Magn. Reson.* 1998, **135**, 144.
118. D. Schaefer, H. W. Spiess, U. W. Suter, and W. W. Fleming, *Macromolecules* 1990, **23**, 3431.
119. A. Hagemeyer, K. Schmidt-Rohr, and H. W. Spiess, *Adv. Magn. Reson.* 1989, **13**, 85.

120. J. J. Titman, Z. Luz, and H. W. Spiess, *J. Am. Chem. Soc.* 1992, **114**, 3756.
121. H. Geen, J. J. Titman, J. Gottwald, and H. W. Spiess, *J. Magn. Reson.* 1995, **A 114**, 264.
122. J. Gottwald, D. E. Demco, R. Graf, and H. W. Spiess, *Chem. Phys. Lett.* 1995, **243**, 314.
123. Demus, D.; Goodby, J. W.; Gray, G. W.; Spiess, H. W.; Vill, V. (eds.) *Handbook of Liquid Crystals*; Wiley-VCH: Weinheim, 1998.
124. Herwig, P.; Kayser, C. W.; Müllen K.; Spiess, H. W. *Adv. Mater.* 1996, **8**, 510.
125. S. P. Brown, X. X. Zhu, K. Saalwächter, and H. W. Spiess, *J. Am. Chem. Soc.* 2001, **123**, 4275.
126. G. A. Jeffrey and W. Saenger, 'Hydrogen Bonding in Biological Structures', Springer-Verlag, New York, 1991.
127. S. P. Brown, I. Schnell, J. D. Brand, K. Müllen, and H. W. Spiess, *Phys. Chem. Chem. Phys.* 2000, **2**, 1735.
128. K. Schmidt-Rohr, J. Clauss, and H. W. Spiess, *Macromolecules* 1992, **25**, 3273.
129. K. Landfester, C. Boeffel, M. Lambla, and H. W. Spiess, *Macromolecules* 1996, **29**, 5972.
130. P. Caravatti, G. Bodenhausen, and R. R. Ernst, *Chem. Phys. Lett.* 1982, **89**, 363.
131. P. Caravatti, L. Braunschweiler, and R. R. Ernst, *Chem. Phys. Lett.* 1983, **100**, 305.
132. B.-J. Van Rossum, H. Förster, and H. J. M. De Groot, *J. Magn. Reson.* 1997, **124**, 516.
133. K. Saalwächter, R. Graf, and H. W. Spiess, *J. Magn. Reson.* 1999, **140**, 471.
134. K. Saalwächter, R. Graf, and H. W. Spiess, *J. Magn. Reson.* 2001, **148**, 398.
135. G. Bodenhausen and D. J. Ruben, *Chem. Phys. Lett.* 1980, **69**, 185.
136. L. Müller, *J. Am. Chem. Soc.* 1979, **101**, 4481.
137. A. Lesage, D. Sakellariou, S. Steuernagel, and L. Emsley, *J. Am. Chem. Soc.* 1998, **120**, 13194.
138. A. Lesage, P. Charmont, S. Steuernagel, and L. Emsley, *J. Am. Chem. Soc.* 2000, **122**, 9739.
139. A. Lesage and L. Emsley, *J. Magn. Reson.* 2001, **148**, 449.
140. R. K. Hester, J. L. Ackerman, B. L. Neff, and J. S. Waugh, *Phys. Rev. Lett.* 1976, **36**, 1081.
141. M. G. Munowitz, R. G. Griffin, G. Bodenhausen, and T. H. Huang, *J. Am. Chem. Soc.* 1981, **103**, 2529.
142. M. G. Munowitz and R. G. Griffin, *J. Chem. Phys.* 1982, **76**, 2848.
143. J. E. Roberts, G. S. Harbison, M. G. Munowitz, J. Herzfeld, and R. G. Griffin, *J. Am. Chem. Soc.* 1987, **109**, 4163.
144. D. McElheny, E. DeVita, L. Frydman, *J. Magn. Reson.* 2000, **143**, 321.
145. M. Hohwy, C. P. Jaroniec, B. Reif, C. M. Rienstra, and R. G. Griffin, *J. Am. Chem. Soc.* 2000, **122**, 3218.
146. B.-J. van Rossum, C. P. de Groot, V. Ladizhansky, S. Vega, H. J. M. de Groot, *J. Am. Chem. Soc.* 2000, **122**, 3465.
147. S. Hediger, PhD Thesis, ETH Zurich, 1997.
148. A. Fechtenkötter, K. Saalwächter, M. A. Harbison, K. Müllen, and H. W. Spiess, *Angew. Chem. Int. Ed. Engl.* 1999, **38**, 3039.
149. X. Feng, Y. K. Lee, D. Sandstrøm, M. Edén, H. Maisel, A. Sebald, and M. H. Levitt, *Chem. Phys. Lett.* 1996, **257**, 314.
150. M. Hong, J. D. Gross, and R. G. Griffin, *J. Phys. Chem. B* 1997, **101**, 5869.
151. C. H. Wu, A. Ramamoorthy, and S. J. Opella, *J. Magn. Reson.* 1994, **A 109**, 270.
152. F. M. Marassi and S. J. Opella, *J. Magn. Reson.* 2000, **144**, 150.
153. D. P. Weitekamp, J. R. Garbow, and A. Pines, *J. Chem. Phys.* 1982, **77**, 2870.
154. K. Schmidt-Rohr, D. Nanz, L. Emsley, and A. Pines, *J. Phys. Chem.* 1994, **98**, 6668.
155. S. Caldarelli, M. Hong, L. Emsley, and A. Pines, *J. Phys. Chem.* 1996, **100**, 18696.
156. B. M. Fung, K. Ermolaev, and Y. Yu *J. Magn. Reson.* 1999, **138**, 28.
157. H. Sun and B. M. Fung *Liq. Crystals* 2000, **27**, 755.
158. S. Massou, M. Tropis, and A. Milon *J. Chim. Phys. Phys.-Chim. Bio.* 1999, **96**, 1595.
159. S. Caldarelli, A. Lesage, and L. Emsley, *J. Am. Chem. Soc.* 1996, **118**, 12224.
160. J. Haase and M. S. Conradi, *Chem. Phys. Lett.* 1993, **287**, 209.
161. A. P. M. Kentgens and R. Verhagen, *Chem. Phys. Lett.* 1999, **300**, 435.
162. Z. Yao, H.-T. Kwak, D. Sakellariou, L. Emsley, and P. J. Grandinetti, *Chem. Phys. Lett.* 2000, **327**, 85.

163. S. Ganapathy, S. Schramm, and E. Oldfield, *J. Chem. Phys.* 1982, **77**, 4360.
164. A. Samoson, E. Lippmaa, and A. Pines, *Mol. Phys.* 1988, **65**, 1013.
165. K. T. Mueller, B. Q. Sun, G. C. Chingas, J. W. Zwanziger, T. Terao, and A. Pines, *J. Magn. Reson.* 1990, **86**, 470.
166. A. Llor and J. Virlet, *Chem. Phys. Lett.* 1988, **152**, 248.
167. I. Farnan, P. J. Grandinetti, J. H. Baltisberger, J. F. Stebbins, U. Werner, M. A. Eastman, and A. Pines, *Nature* 1992, **358**, 31.
168. P. J. Grandinetti, in 'Encyclopedia of Nuclear Magnetic Resonance', eds. D. M. Grant and R. K. Harris, Wiley, Chichester, 1996, Vol. 3, p.1768.
169. L. Frydman and J. S. Harwood, *J. Am. Chem. Soc.* 1995, **117**, 5367.
170. S. P. Brown and S. Wimperis, *J. Magn. Reson.* 1997, **128**, 42.
171. T. Vosegaard, P. Florian, P. J. Grandinetti, and D. Massiot, *J. Magn. Reson.* 2000, **143**, 217.
172. M. Pruski, J. W. Wiench, and J.-P. Amoureux, *J. Magn. Reson.* 2000, **147**, 286.
173. J. Rocha, A. P. Esculas, C. Fernandez, and J.-P. Amoureux, *J. Phys. Chem.* 1996, **100**, 17889.
174. P. J. Dirken, S. C. Kohn, M. E. Smith, and E. R. H. van Eck, *Chem. Phys. Lett.* 1997, **266**, 568.
175. Z. Xu, H. Maekawa, J. V. Oglesby, and J. F. Stebbins, *J. Am. Chem. Soc.* 1998, **120**, 9894.
176. S. P. Brown, S. E. Ashbrook, and S. Wimperis, *J. Phys. Chem. B* 1999, **103**, 812.
177. S. Caldarelli and F. Ziarelli, *J. Am. Chem. Soc.* 2000, **122**, 12015.
178. L. B. Alemany, R. L. Callender, A. R. Barron, S. Steuernagel, D. Iuga, and A. P. M. Kentgens, *J. Phys. Chem. B* 2000, **104**, 11612.